Precambrian Research 394 (2023) 107114

Contents lists available at ScienceDirect

Precambrian Research

journal homepage: www.elsevier.com/locate/precamres

Paleogeography and high-precision geochronology of the Neoarchean Fortescue Group, Pilbara, Western Australia

Jennifer Kasbohm [a,1,*], Blair Schoene [a], Scott A. Maclennan [a,2], David A.D. Evans [b], Benjamin P. Weiss [c]

[a] Department of Geosciences, Princeton University, Princeton, NJ 08544, USA
[b] Department of Earth & Planetary Sciences, Yale University, New Haven, CT 06511, USA
[c] Department of Earth, Atmospheric, and Planetary Sciences, Massachusetts Institute of Technology, Cambridge, MA 02139, USA

ARTICLE INFO

Keywords:
Paleomagnetism
Archean tectonics
U-Pb zircon geochronology
Large igneous provinces
Magnetic field reversals

ABSTRACT

While rates of Phanerozoic plate movements and magnetic field reversals have been well studied, little is known about such phenomena on early Earth. The ca. 2.8–2.7 Ga Fortescue Group on the Pilbara craton in Western Australia has been recognized as a well-preserved sequence of Archean rift volcanics thought to derive from a flood basalt province, and may have been moving rapidly across the globe at two different intervals in its depositional history. We present the results of a magnetostratigraphic study integrated with high-precision U-Pb ID-TIMS geochronology aiming to quantify rates of cratonic motion and provide a continuous time series for changes in Pilbara paleogeography during these two rapid intervals, at ~2.77 and 2.72 Ga. We provide six new or updated high-quality paleomagnetic poles for inclusion in databases tracking Precambrian cratonic motion. During the craton's largest geographic displacement at ~2.77 Ga, we resolve a minimum drift rate of 23 ± 20 cm/a if there was substantial rotation of the Pilbara craton along with translational motion, and a more rapid minimum estimate of 64 ± 23 cm/a if the motion was dominated by translation; these estimates exceed both Mesoarchean and most modern rates of plate motion. We provide a new high-precision U-Pb zircon age of 2721.23 ± 0.88/0.88/6.9 Ma for the Tumbiana Formation stromatolite colony, which developed as the Pilbara craton drifted from 51.5 ± 7.0° to 32.1 ± 5.7° paleolatitude. Although the Fortescue Group has been considered an early prototype of large igneous provinces, it was emplaced over a longer duration than its Phanerozoic counterparts and does not fit at least one definition of a large igneous province (LIP). But as a potential prototype of LIP magmatism, the Fortescue succession chronicles eruptive dynamics, rapid paleogeographic changes, and a series of robustly determined magnetic field reversals during the Neoarchean.

1. Introduction

The acceptance of plate tectonics irreversibly changed the way geoscientists understand Earth's mantle dynamics and lithospheric movements. However, a point of contention in the study of Earth history is whether plate tectonic processes were operating during the Archean (Brown et al., 2020), and if so, whether they were fundamentally different from those of the present. Did a hotter Earth allow for more vigorous convection and rapid plate motion (Davies, 1992), or were tectonics slowed by dehydration and thickening of the mantle lithosphere (Korenaga, 2003)? Furthermore, determining the timing and frequency of magnetic field reversals during the Archean is hampered not only by the paucity of rocks from this eon, but also by the required retention of a primary magnetic signature, the ability to obtain age constraints, and the preservation of somewhat continuous sequences that document multiple polarity intervals, leading to only sparse documentation of these events (Gallet et al., 2012; Hulot et al., 2010, and references therein).

A paleomagnetic study integrated with high-precision geochronological data (e.g., Swanson-Hysell et al., 2019) has the potential to

* Corresponding author.
E-mail addresses: jennifer.kasbohm@yale.edu (J. Kasbohm), bschoene@princeton.edu (B. Schoene), scott.maclennan@wits.ac.za (S.A. Maclennan), david.evans@yale.edu (D.A.D. Evans), bpweiss@mit.edu (B.P. Weiss).
[1] Present address: Department of Earth & Planetary Sciences, Yale University, New Haven, CT 06511, USA.
[2] Present address: School of Geosciences, University of the Witwatersrand, Johannesburg, South Africa.

https://doi.org/10.1016/j.precamres.2023.107114
Received 9 September 2022; Received in revised form 1 June 2023; Accepted 2 June 2023
Available online 19 June 2023

quantify rates of plate motion during the Archean. Collecting both paleomagnetic and geochronological samples within a detailed stratigraphic context may provide a continuous time series for changes in paleogeography, and removes the need for regional correlation. Continental flood basalts are ideal targets for this type of study because basalt is a faithful paleomagnetic recorder that retains a record of paleohorizontal and is erupted in a layered stratigraphic manner.

The ca. 2.8–2.7 Ga Fortescue Group of the Pilbara craton in Western Australia (Fig. 1) has been recognized as one of the oldest and best-preserved Archean flood basalt successions hypothesized to be sourced from a continental rift (Blake, 1993), with an estimated basaltic volume of 250,000 km^3 (Thorne & Trendall, 2001). The Fortescue succession has the potential to yield insights not only into the rate of cratonic motion occurring in the Archean, but also into how these processes may have affected evolving life on Earth prior to the Great Oxidation Event. The Fortescue Group has been subject to prior lithological (Thorne & Trendall, 2001), geochronological (Blake et al., 2004), and paleomagnetic study (Strik, 2004; Strik et al., 2003) that suggest its suitability for a detailed stratigraphic approach (Fig. 1b).

Blake (2001) divided the Fortescue Group into 12 unconformity-bounded packages, which were later dated with SHRIMP U-Pb zircon geochronology (Blake et al., 2004). Guided by Blake's stratigraphic framework, Strik et al. (2003) published the first detailed Fortescue Group paleomagnetic study, which yielded an apparent polar wander path for the ca. 60 Myr depositional history of the group and the earliest stratigraphically documented reversal in Earth's geomagnetic field. There are two intervals in the Fortescue Group where the Pilbara craton appears to have been moving rapidly (Strik, 2004; Strik et al., 2003). However, analytical errors on the order of millions of years for the current ages for the Fortescue Group inhibit the calculation of Pilbara drift rates in the short time span of these potentially rapid intervals. Additionally, the difficulty in correlating rocks from distant regions of the Fortescue Group (Fig. 1) precludes the possibility of integrating the current paleomagnetic and geochronological datasets.

Presented here are the results of an integrated stratigraphic, paleomagnetic, and geochronological study aiming to quantify the minimum velocity of the Pilbara during these two intervals of potentially rapid motion. We present six new or updated high-quality paleomagnetic poles for the Fortescue Group. With four new high-precision U-Pb CA-ID-TIMS ages, we provide improved velocity constraints that exceed both modern and Mesoarchean drift rates. We show that the Tumbiana stromatolite colony developed 2721.23 ± 0.88/0.88/6.9 million years ago as the Pilbara craton drifted from 51.5 ± 7.0° to 32.1 ± 5.7° paleolatitude. Finally, we revisit the classification of the Fortescue Group as a large igneous province, and comment on its history of magnetic field reversals. Whether or not the Fortescue Group meets the criteria for classification as a large igneous province, it can provide numerous insights into the tectonics, magmatism, and state of the geodynamo of the Archean Earth system.

2. Geologic context

The Fortescue Group is a ~6 km thick succession comprising flood basalts, mafic tuffs, felsic volcanics, and clastic sedimentary rocks currently exposed over 40,000 km^2 of the Pilbara craton. It unconformably overlies 3.5–2.9 Ga granite-greenstone basement rocks (Thorne & Trendall, 2001). The Fortescue Group was deformed into numerous synclines, but at most was metamorphosed to the prehnite-pumpellyite-epidote phase (Blake et al., 2004). The Fortescue succession is divided into the lower Nullagine Supersequence and the Upper Mount Jope Supersequence (Fig. 1b), each thought to represent a phase of continental rifting (Blake, 1993). Blake (2001) later divided these supersequences into 12 unconformity-bound packages. Even though unconformities are decreasingly obvious higher in the Fortescue Group stratigraphy (lacking obvious changes in bedding or lithology, or signs of erosion), significant time gaps were inferred between each package (Blake, 2001).

The onset of Fortescue Group deposition, beginning with the Nullagine Supersequence, occurred in geographically disconnected fault-bounded basins (Blake, 1993). The earliest Fortescue Group strata are found only in the Marble Bar Basin, as a thin braided fluvial sedimentary succession overlain by thick subaerial basalts of Package 0 (as classified by Strik, 2004). A more extensive succession of basalts covered the entire northern Pilbara craton, known as Package 1 (Strik et al., 2003; Blake et al., 2004). Most published literature, including bedrock geologic map quadrangles (e.g., Hickman, 2010) combine both Packages 0 and 1 into the single lithostratigraphic designation "Mount Roe Basalt" despite the two subsets' profound differences in degree of deformation (Blake, 1984) and paleomagnetic signature (Strik, 2004). Evans et al. (2017) discuss the regional stratigraphic implications of this distinction. The Mount Roe Basalts are followed by a mostly clastic sedimentary unit, usually designated as the Hardey Formation, which also contains a felsic porphyry and minor mafic volcanic components (Packages 2–4; Blake, 2001). The Mount Jope Supersequence begins with the subaerial Kylena Basalt (Packages 5–6), which gives way to the volcaniclastic and carbonate rocks of the Tumbiana Formation (Package 7), followed by emplacement of the Maddina Basalt (Packages 8–10), and ultimately, marine sediments of the Jeerinah Formation (Packages 11–12).

While the entire Fortescue Group underwent regional subsidence, increased crustal thinning in the southern part of the craton led to coastal depositional environments and subaqueous volcanism, in contrast to continued subaerial conditions in the northern Pilbara (Thorne & Trendall, 2001). Four mafic dyke suites (Black Range, Mount Maggie, Five Mile Creek, and Castle Creek) have been geochemically and paleomagnetically correlated to the Fortescue Group (Strik et al., 2003). While the Fortescue Group is suggested to be one of Earth's oldest continental flood basalts, with an estimated volume of 250,000 km^3, its long duration of emplacement and varied geologic record including major sedimentary units may complicate that assessment, despite the physical resemblance of its basaltic packages to other Phanerozoic large igneous provinces (Thorne & Trendall, 2001).

Determining a rate of plate motion for the Pilbara craton during the Neoarchean has been dependent on findings from geochronology and paleomagnetism. When first described, the Fortescue Group was identified as Proterozoic, since it lacked the metamorphic grade and structural complexity characteristic of most Archean successions (Blake, 2001). The first attempt to date the group with a Rb-Sr whole rock isochron yielded an age of 2124 ± 195 Ma (Trendall, 1975). The first conventional zircon age for the Fortescue Group was 2768 ± 13 Ma (upper intercept), for the Package 2 Spinaway Porphyry (Pidgeon, 1984). Arndt et al. (1991) produced the first suite of sensitive high-resolution ion microprobe (SHRIMP) zircon U-Pb ages for the Fortescue Group, which ranged from 2775 ± 10 Ma for a felsic volcanic rock near the base of the Mount Roe Basalt to 2684 ± 6 Ma for an ignimbrite member of the Jeerinah Formation. Blake et al. (2004) produced 11 higher-precision SHRIMP zircon ages for the Fortescue, ranging from 2766 ± 2 Ma for the Spinaway Porphyry to 2715 ± 2 Ma for a reworked felsic tuff in Package 11, yet dates obtained for a number of packages overlapped within analytical uncertainty. There are no reliable age constraints on Package 0 because it has been defined only on the basis of its paleomagnetic direction, and none of the aforementioned dates derive confidently from a site with Package 0 paleomagnetic affinity (summarized by Evans et al., 2017). Without precise age constraints, rates of motion for the Pilbara craton could not be calculated during the intervals when Strik (2004) observed 70° of movement in the paleomagnetic poles between Package 0 and 1, and 14.4° of movement across the Package 7–8 boundary.

3. Methods

Two field seasons in summers 2013 and 2014 were undertaken in the Fortescue Group, in which stratigraphic sections were measured and

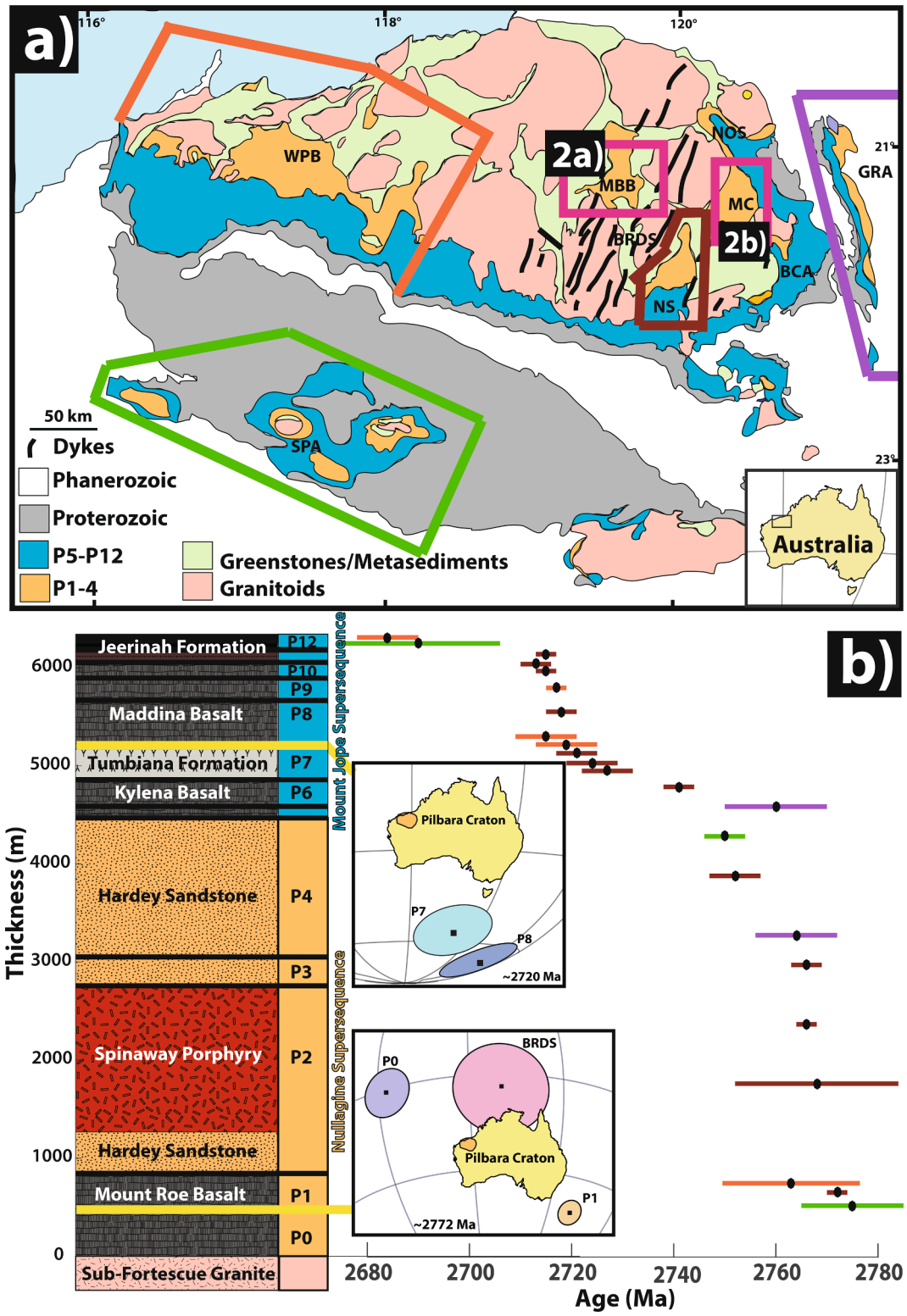

Fig. 1. Geologic context of the Fortescue Group as known prior to this study. The areal extent of the Fortescue Group is shown in (a) (after Blake et al., 2004), with abbreviations for the following regions: WPB – West Pilbara Basin; MBB – Marble Bar Basin; NS – Nullagine Syncline; MC – Meentheena Centrocline; GRA – Gregory Range Area; SPA – Southwest Pilbara Area; BCA – Boodalyeri Creek Area; NOS – North Oakover Syncline; BRDS – Black Range Dyke Swarm. Prior work on the stratigraphy (Thorne & Trendall, 2001), paleomagnetism (Evans et al., 2017; Strik, 2004), and geochronology (Blake et al., 2004, and references therein) is summarized in (b). The colored error bars for geochronology correspond to outcrop areas outlined in (a). Yellow lines indicate the two intervals of Fortescue stratigraphy discussed in this paper, between Packages 0 and 1 and Packages 7 and 8. (For interpretation of the references to color in this figure legend, the reader is referred to the web version of this article.)

sampled at four different localities. Two sections were measured at dm-scale across the Package 0–1 boundary at Glen Herring Gorge (GHG; 900 m) and Coongan River (CR; 900 m) (Fig. 2a). For Packages 7–8, two sections were measured on opposite sides of the Meentheena Centrocline (Fig. 2b); the Meentheena Centrocline North (MCN) section was 900 m thick, while the Meentheena Centrocline South (MCS) section had a thickness of 600 m. Unit thicknesses and lithologies, as well as the stratigraphic positions of paleomagnetism sample sites and geochronology samples, were recorded in each section (Fig. 3).

3.1. Paleomagnetism

Eight hundred forty-six paleomagnetic cores were drilled from 75 sites, and oriented by magnetic and solar compasses. Most sites were single stratigraphic horizons (lava flows) with 5–10 samples collected, but JK1321, JK1328, and JK1417 consist of multiple stratigraphic heights with 1–2 samples per horizon in sections of 52, 95 and 18 m, respectively. Three sites, JK1315 (GHG Package 1 hyaloclastite breccia), JK1407 (GHG Package 0 basal conglomerate), and JK1435 (CR Package 1 hyaloclastite breccia), each consist of 20 clasts sampled for conglomerate tests on the age of paleomagnetic remanence (Watson, 1956). No significant deviation of magnetic declination from the regional average (1.7°) was observed in any of the sites sampled.

Samples were trimmed to ~10 cm^3 specimens and analyzed at the MIT Paleomagnetism Laboratory using a cryogenic DC-SQuID magnetometer (sensitivity with sample holder ~10^{-9} Am^2) with automated sample changer (Kirschvink et al., 2008). NRM measurements were followed by a liquid nitrogen, low-temperature demagnetization step, and underwent alternating field (AF) demagnetization at steps of 0, 2.5, 5, 7.5, and 10 mT. Samples then were subjected to ~20 successive high-temperature demagnetization steps of decreasing intervals up to 600 °C, when measurements' intensity decreased by two orders of magnitude. Typical demagnetization steps were 100, 200, 250, 300, 350, 400, 450, 480, 500, 520, 530, 540, 550, 560, 568, 575, 580, 585, 590, 595, and 600 °C. Each sample's magnetic components were resolved with principal component analysis (Kirschvink, 1980), using software created by Jones (2002) — least-squares fits were applied to successive demagnetization steps that represented the characteristic remanent magnetization (ChRM) of each sample. These linear fits were anchored to the origin in all cases because there is no evidence for additional components prior to total demagnetization, which we performed through at least two extra heating steps per sample. All lines with mean angular deviation (MAD) >10° were omitted from locality means. Mean declination (D), inclination (I), precision parameters (k), and 95% confidence limits (α95) were calculated to find the average ChRM of each sampling site using Fisher (1953) statistics and are published in Table S1. All site mean directions described in the text below and documented in the figures are in tilt-corrected coordinates.

3.2. Geochronology

Twenty-one interflow units were logged and collected as potential geochronology samples in all Package 0–1 and 7–8 stratigraphic sections, and from the Package 2 Spinaway Porphyry. Four samples yielded zircons of Neoarchean age (~2.7 Ga). Geochronology methods are as described in Kasbohm & Schoene (2018) and are reproduced here.

3.2.1. Zircon separation and preparation

Zircons were separated from their host rock through standard methods of crushing, gravimetric-, and magnetic-separation techniques using a Bico Braun "Chipmunk" Jawcrusher, disc mill, hand pan, hand magnet, Frantz isodynamic separator, and methylene iodide. Zircons from the least magnetic and most dense mineral separate were transferred in bulk to quartz crucibles and annealed in a muffle furnace at 900 °C for 48 h after Mattinson (2005). After annealing, 20–40 zircon grains from each sample were photographed and picked in reagent-grade ethanol for analysis. Euhedral grains with a range of morphologies were selected, while those with visible cracks, inclusions, and

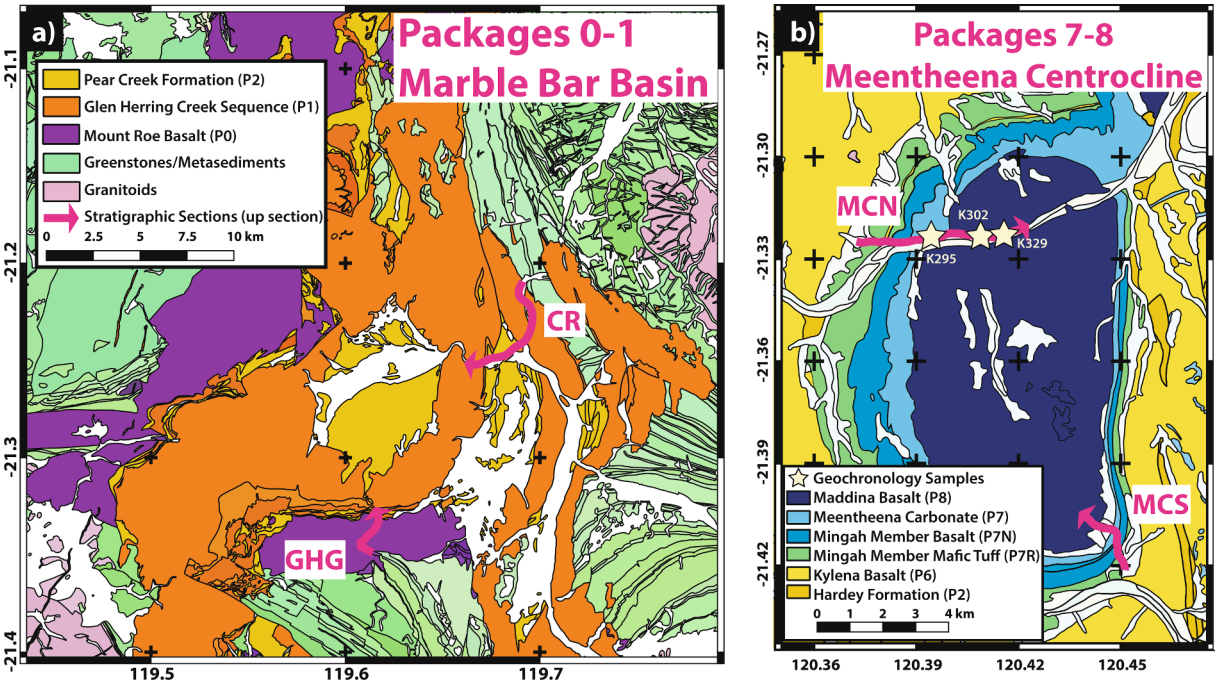

Fig. 2. Regional maps with stratigraphic sections. The Glen Herring Gorge (GHG) and Coongan River (CR) Package 0–1 stratigraphic sections were measured in the Marble Bar Basin, as seen on the geologic map in (a). Correlations of Package 0–1 stratigraphic units were guided by the radiometry mapping of Van Kranendonk et al. (2004). Package 7–8 stratigraphic sections were measured in the Meentheena Centrocline, with North (MCN) and South (MCS) sections highlighted in (b). Stratigraphic sections are highlighted in pink, with the arrowhead indicating the direction of upward in stratigraphy. (For interpretation of the references to color in this figure legend, the reader is referred to the web version of this article.)

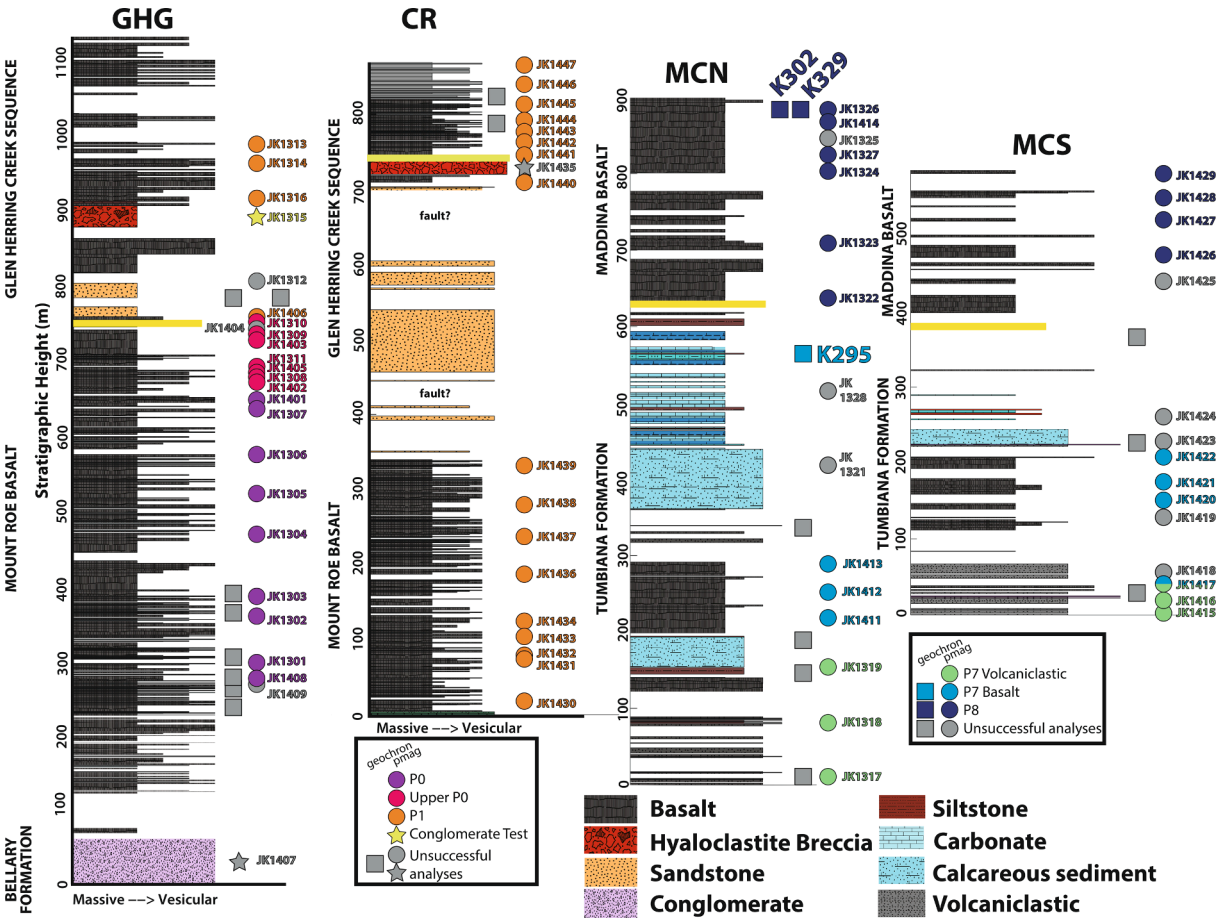

Fig. 3. Measured stratigraphic sections. Four stratigraphic sections were measured in the Fortescue Group and are displayed here, with lithological legend and positions of paleomagnetic sample sites (circles for regular sites, stars for conglomerate tests) and geochronology samples (squares), color-coded by paleomagnetic directional group. The width of the stratigraphic units corresponds to an increasing quantity of vesicles for basalts, and increased grain size for sediments, as described in the text. Grey circles indicate paleomagnetic sites not included in site means due to present day field overprints, scattered directions, or failed conglomerate tests; grey squares indicate interbeds sampled that either did not yield zircons or yielded inherited zircons. Yellow lines indicate proposed package boundaries. (For interpretation of the references to color in this figure legend, the reader is referred to the web version of this article.)

cores were avoided. Individual grains were transferred using stainless steel picking tools into separate 3-mL Savillex Hex beakers containing distilled acetone and taken to the clean lab for analysis.

3.2.2. U-Pb zircon ID-TIMS analysis

Single zircon grains were loaded into 200 uL Savillex "micro"-capsules with 100 μL 29 M HF + 15 μL 3 N HNO_3 for a single leaching step in high-pressure Parr bombs at 185 °C for 12 h to remove crystal domains affected by Pb-loss (Mattinson, 2005). Grains were rinsed post-leaching in 6 N HCl, MQ H2O, 3 N HNO_3, and 29 M HF prior to spiking with EARTHTIME ^{205}Pb-^{233}U-^{235}U tracer and addition of 100uL 29 M HF + 15 μL 3 N HNO_3 (Condon et al., 2015; McLean et al., 2015). Zircons were then dissolved to completion in Parr bombs at 210 °C for 48 h. Dissolved zircon solutions were subsequently dried down, dissolved in 100 μL 6 N HCl, and converted to chlorides in Parr bombs at 185 °C for 12 h, after which solutions were dried again and brought up in 50 μL 3 N HCl. The U-Pb and trace element aliquots were then separated by anion exchange chromatography using 50 μL columns and AG-1 X8 resin (200–400 mesh, chloride from Eichrom) (Krogh, 1973), and dried down with a microdrop of 0.015 M H_3PO_4. The dried U and Pb aliquot was loaded in a silica gel emitter (Gerstenberger & Haase, 1997) to an outgassed zone-refined Re filament.

Isotopic determinations were performed using an Isotopx Phoenix62 thermal ionization mass spectrometer (TIMS) at Princeton University, with Pb analysis performed in peak-hopping mode on a Daly-photomultiplier ion-counting detector. A correction for mass-dependent Pb fractionation was applied using a Pb fractionation of 0.182 ± 0.041%/amu, as determined by repeat measurements of NBS 982 at Princeton. Daly-photomultiplier deadtime was monitored, as determined by repeat measurements of the NBS 982 standard. Corrections for interfering isotopes under masses 202, 204, and 205 were made cycle-by-cycle by measuring masses 201 and 203 and assuming they represent $^{201}BaPO_4$ and ^{203}Tl and using natural isotopic abundances to correct for $^{202}BaPO_4$, $^{204}BaPO_4$, $^{205}BaPO_4$, and ^{205}Tl.

UO_2 measurements were performed in static mode on Faraday cups with a bulk U fractionation correction calculated from the deviation of measured $^{233}U/^{235}U$ from the known tracer $^{233}U/^{235}U$ (0.995062 ± 0.000054 (1σ)), and an oxide composition of $^{18}O/^{16}O$ of 0.00205 was used (Nier, 1950). Data reduction was performed using the programs Tripoli and U-Pb Redux (Bowring et al., 2011; McLean et al., 2011) and the decay constants of Jaffey et al. (1971). All Pbc was attributed to laboratory blank with a mean isotopic composition determined by total procedural blank measurements (see Table S2 for values). Two different blank corrections are applied; Pre-Side Filaments (PSF) was used for measurements made prior to January 2018, when the lab began routinely heating side filaments prior to analyses, and Side Filaments (SF) for measurements made after. Uncertainties in reported individual U-Pb zircon dates are at the 95% confidence level, excluding tracer

calibration and decay constant uncertainties. Our U-Pb sample ages are reported with 2σ uncertainties ± x/y/z, where x represents analytical uncertainty alone, y includes uncertainties in the ET-535 tracer used, and z includes all systematic uncertainties. Correction for initial ^{230}Th disequilibrium in the ^{206}Pb/^{238}U system was made on a fraction-by-fraction basis by estimating $(Th/U)_{magma}$ using $(Th/U)_{zircon}$ determined by TIMS and a mean $(Th/U)_{zircon\text{-}magma}$ partition coefficient ratio of 0.19 ± 0.11, which encompasses the range of values for $(Th/U)_{zircon\text{-}magma}$ partition coefficients obtained from glasses from a variety of volcanic settings (Claiborne et al., 2018). Uncertainties for the resulting $(Th/U)_{magma}$ were also calculated on a fraction-by-fraction basis, propagating the uncertainty in the $(Th/U)_{zircon\text{-}magma}$ partition coefficient. For inherited zircons, we use a uniform $(Th/U)_{magma}$ value of 2.8 for this correction (Table S2).

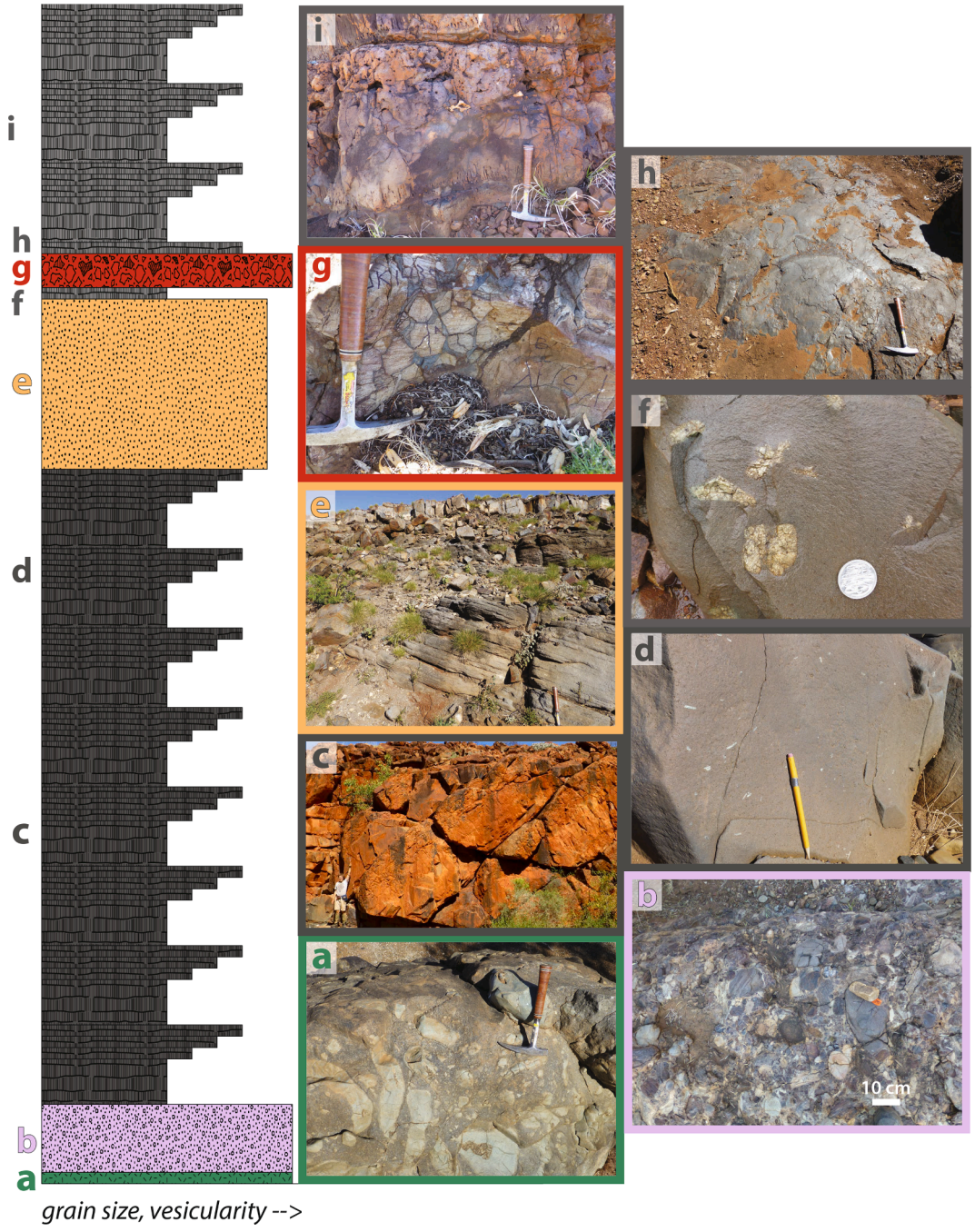

Fig. 4. Schematic stratigraphy of Packages 0–1. This schematic stratigraphic column (not to vertical scale) shows the lithologies present across the Package 0–1 boundary, which is located between d and e. Photos from different field localities illustrate each representative stratigraphic interval. **(A)** The base of the Fortescue Group has an unconformable contact with the Paleoarchean Warrawoona Group; the Apex Basalt at CR is pictured here. **(B)** The Bellary Formation conglomerate is the oldest depositional unit in the Fortescue Group; it is pictured here at GHG. **(C)** A succession of Package 0 lava flows observed at the Pear Creek Centrocline. **(D)** Cm-scale plagioclase laths in a Package 0 massive basalt flow. **(E)** Basal Package 1 sediments at Pear Creek Centrocline. **(F)** Package 1 plagioclase glomerocrysts observed at GHG. **(G)** Package 1 hyaloclastite breccia sampled for conglomerate tests, pictured here at GHG. **(H)** Package 1 pillow basalts at Pear Creek Centrocline. **(I)** Package 1 lava flows, with basal pipe vesicles, vesicular flow tops, and distinct flow boundaries at CR. For measured stratigraphic sections, please refer to Fig. 3.

4. Results

4.1. Volcanostratigraphy

For all Fortescue Group lava flows observed, most lava flows contain pipe vesicles at the base, followed by a massive interval that typically constitutes most of each flow's thickness and frequently contains isolated bands of vesicles or pods of vesicles, interpreted as representing paths of volatile escape during cooling (Thorne & Trendall, 2001). Above the massive interior of the flow, the unit becomes increasingly vesicular until the most vesicular flow top, in which vesicles are either scattered randomly or aligned in bedding-parallel sheets. In each measured section, three categories of vesicularity were identified (1 V=<25%, 2 V = 25–50%, 3 V=>50%), corresponding to the width of stratigraphic intervals in Fig. 3. Many lava flows contained sub-mm plagioclase and pyroxene phenocrysts, and a subset of these exhibited mm-cm scale plagioclase phenocrysts seen singularly or in a glomeroporphyritic array. Some lava flows were overlain by thin glassy sedimentary interbeds, sampled as potential ash beds.

4.1.1. Packages 0–1: Mount Roe Basalt

The lowermost part of the Fortescue stratigraphy has an unconformable boundary with the underlying granite-greenstone terrain (Fig. 4a). At GHG, the Fortescue overlies the Duffer Formation, and at CR, it overlies the Apex Basalt; these are members of the greenstone-grade Warrawoona Group, with ages ranging within 3525–3426 Ma (Van Kranendonk et al., 2007). The lowest unit in the Fortescue stratigraphy, the Bellary Formation, is the base of the section at GHG (Fig. 3), consisting of ~60 m of silicified, coarse-grained quartz-ofeldspathic sandstone and conglomerate, with cm–dm scale clasts of

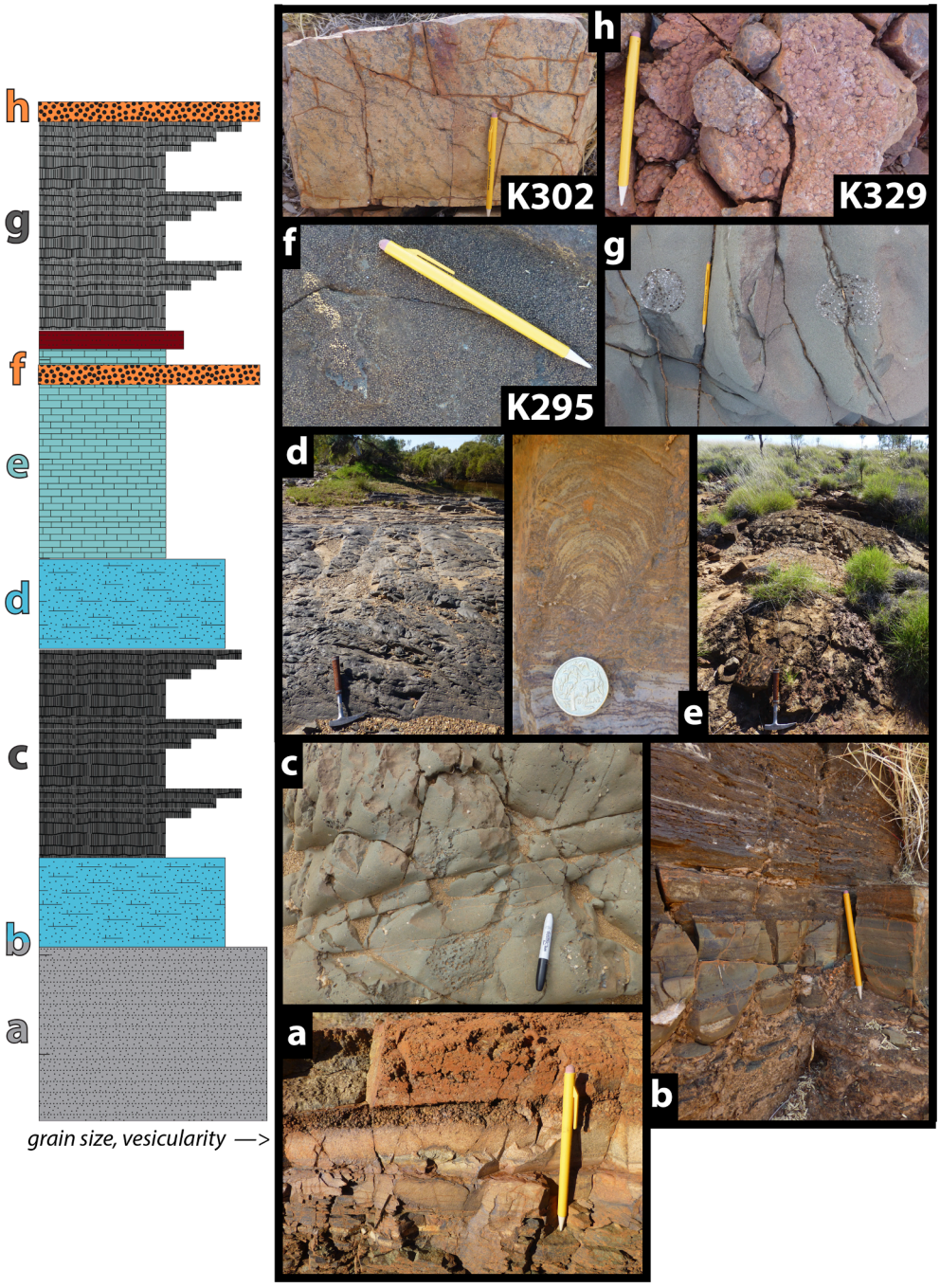

Fig. 5. Schematic stratigraphy of Packages 7–8. This schematic stratigraphic column (not to vertical scale) shows the lithologies present across the Package 7–8 boundary, which is located between f and g. All photos are from MCN. **(A)** Mafic volcaniclastic sediments with interbedded lapilli at the base of Package 7. **(B)** Contact of mafic volcaniclastics with interval of calcareous sediments and microbialites. **(C)** Package 7 massive basalt flow with vesicle pods and bands. **(D)** Calcareous sandstone with cross-beds in foreground. **(E)** Cm- and m- scale Tumbiana stromatolites. **(F)** Lapilli tuff interbedded with stromatolites, sampled for geochronology as K295. **(G)** Package 8 massive basalt flow with vesicle cylinders. **(H)** Lapilli tuff overlying Package 8 lava flows, sampled for geochronology at two different locations, K302 and K329.

banded iron formation and sediments (Fig. 4b); this unit is up to 500 m thick elsewhere in the Marble Bar Basin (Blake, 1984). The mode of deposition for the formation is interpreted as a braided fluvial environment (Blake, 1993). The next stratigraphic unit at GHG comprises 76 lava flows of the Mount Roe Basalt (Fig. 4c), with some flows featuring sparse cm-long needle-like plagioclase phenocrysts (Fig. 4d); 51 lava flows were measured in the lower portion of the CR section (see further detail below).

In the Marble Bar Basin, Package 1 of Strik (2004) corresponds to the Glen Herring Creek Sequence of Blake (1984). The basal unit of the sequence is ~ 100 m of coarse-grained sandstone to gritstone, with cross beds occasionally present and showing north-to-south flow directions (Fig. 4e). Above the sandstone, a distinctive 10 m basalt flow with plagioclase glomerocrysts was observed at GHG and CR (Fig. 4f), followed by 30 m of a hyaloclastite breccia (Fig. 4g) and a few meters of pillow basalts (Fig. 4h), indicating a brief interval of subaqueous eruption. Subaerial basaltic lava flows return after these basal units, some with cm-scale pipe vesicles at their bases (Fig. 4i); 18 lava flows were measured at GHG, through the end of available basalt outcrop, and 17 lava flows were measured at CR, though basalt flows continued above the end of the measured section.

4.1.2. Packages 7–8: Tumbiana Formation & Maddina Basalt

Stratigraphic sections were measured across the Package 7–8 transition at MCN and MCS (Fig. 3); field photos from MCN are in Fig. 5. Package 7 lithostratigraphically corresponds to the Tumbiana Formation, comprising the basal Mingah Member volcaniclastics with minor subaerial lava flows overlain by the Meentheena Member carbonates and stromatolites. MCN is the Pelican Pool type section where Lipple (1975) first described the members of the Tumbiana Formation. The lowest unit observed in the field is 150 m of fine- to medium-grained basaltic sandstone (Fig. 5a), recognized as a mafic tuff (Blake, 2001). Weathered units of this sediment are marked by mm-scale vugs, while more coherent beds exhibit cross beds, teepee structures, and desiccation cracks. Accretionary lapilli of 2–10 mm diameter are prominently interbedded in the mafic tuff, either deposited in layers of cm–dm scale thickness or filling hollows such as desiccation cracks. Lapilli show an internally concentric structure and are interpreted as primary pyroclastic fall deposits from subaerial hydroclastic eruptions (Thorne & Trendall, 2001). Grain size sorting of the lapilli varies from well- to poorly-sorted and lapilli layers were sometimes observed to be reverse-graded.

Above the mafic tuff, at MCN, minor microbialite layers were observed (possibly under recent cover at MCS; Fig. 5b), followed by three coherent subaerial basalt flows observed at both sections (Fig. 5c). As in Package 0, the flows exhibit a massive base and vesicular top, but are substantially thicker than the Mount Roe Basalt flows (~30 m each in Package 7, rather than < 10 m). The flows are aphryic and sometimes contain cm-scale pipe vesicles at their bases. The basalts are followed by cover (with a coherent bed of lapilli observed in both sections), and then by the Meentheena Member calcareous sediments (mostly under cover at MCS). This unit begins with spheroidally-weathering calcareous sandstone, which becomes cross-bedded with a north-to-south flow direction at the meter scale up-section (Fig. 5d). The sandstone is overlain by carbonate grainstone with laminated or ripple bedding. Climbing ripples and minor interbedded silt layers were observed in the carbonate. Stromatolites range from cm–m scale in diameter and were observed with both columnar and domal morphologies (Fig. 5e). A layer of well-sorted mm-scale lapilli was found near the top of the carbonate succession in both sections and may serve as a stratigraphic tie-point; it was sampled for geochronology at MCN (K295; Fig. 5f). Carbonates and stromatolites were sampled approximately every 50 cm for stable isotope analysis; a detailed measured section and $\delta^{13}C$, $\delta^{18}O$, and $\delta^{44/40}Ca$ results are reported in Blättler et al., (2017). After a small amount of cover, the Package 8 Maddina Basalt begins to outcrop.

The 200–300 m of Maddina Basalt outcropping at MCN and MCS consists of subaerial flows ranging from massive to vesicular textures, as with the other basalts described above. The massive portions of the flows commonly contain dm-scale vesicle cylinders (Fig. 5g). At both MCN and MCS, the first Maddina Basalt flows are coarse-grained with visible sub-mm pyroxene phenocrysts (identified as augite in petrographic studies (Thorne & Trendall, 2001)). An interbedded accretionary lapilli unit overlies the uppermost measured flow at MCN and was sampled for geochronology (K302 and K329, described below; Fig. 5h); no lapilli tuffs were found interbedded with Package 8 lava flows at MCS.

4.2. Paleomagnetism

The stratigraphic positions of paleomagnetic sample sites are plotted with circles on Fig. 3. All site-mean directions and directional groups are provided in Table S1, with equal-area plots of paleomagnetic data for each directional group in Figure S1, using tilt-corrected coordinates. Table 1 summarizes mean paleomagnetic poles calculated for this study and evaluates them against the quality criteria of Van der Voo (1990) and the reliability criteria of Meert et al. (2020).

Since most sandstone and all but seven basalt samples lost remanence at or below 580 °C, the primary magnetic mineral is inferred to be magnetite. The remaining samples, all from conglomerate test sample site JK1407 in the Bellary Formation, and from basalt sample site JK1429 in the Maddina Basalts, lost signal between 600 and 675 °C and are thus interpreted to contain hematite. Site JK1407 exhibits directions overprinted to the present local field at both magnetite and hematite unblocking temperatures. However, we interpret the hematite unblocking temperatures found in seven of the samples in JK1429 to have formed during initial emplacement, since the hematite component gives the same direction as the magnetite component for each sample, and the same direction as the magnetite component in the remaining samples that lack a hematite component. Carbonate samples lost remanence at or below 340 °C, suggesting pyrrhotite as the primary magnetic mineral.

4.2.1. Packages 0–1: Mount Roe Basalt

For the most part, samples from Packages 0 and 1 exhibited excellent stability to thermal demagnetization, with predominantly single-component behavior, though some Package 0 samples exhibited a low-temperature component removed by 400 °C (Fig. 6). Unblocking temperatures were consistently high, mostly between 550 and 580 °C. Samples were generally well-clustered within each locality, and three directional groups emerged from the two sections sampled; site means for the sites included in these groups are plotted in Fig. 7a.

The lowermost basalts at GHG (0–650 m in stratigraphic height) yielded a mean ChRM direction (northwest and moderately down) that broadly agrees with the Package 0 designation of Strik (2004). A conglomerate test on the section's basal Bellary Formation conglomerate fails, with clustered directions around the present-day field (Fig. 8a). Such a test merely indicates local overprinting at that particular site and does not invalidate the positive fold test on Package 0 Basalts across the Marble Bar Basin (Strik, 2004). The retention of unique directions for Packages 0 and 1 also indicates that no regional remagnetization occurred in the studied area. A site-level Lower Package 0 pole, including our new sites and sites sampled in GHG by Strik (2004), is calculated at 04.4°N, 089.9°E, $A_{95} = 6.7°$, paleolatitude = 50.8° (14 sites, 85 samples; Fig. 9).

Samples collected at GHG between 650 and 752 m were found to exhibit a different direction, with declination north and east, and steep downward inclination. The direction appears transitional between that of Lower Package 0 and Package 1. Sites from this portion of GHG are grouped into an Upper Package 0 site-level pole calculated at 08.3°S, 115.6°E, $A_{95} = 13.7°$, paleolatitude = 76.3° (7 sites, 65 samples).

Package 1 directions were observed at GHG beginning at 756 m, below the outcrop of sandstone, and continue through the top of the section. A conglomerate test on clasts of a hyaloclastite breccia at 904 m

Table 1
Summary data for virtual geomagnetic poles. This table summarizes the paleomagnetic poles calculated for this study, compared with data from existing poles, along with ages and quality criteria (#1–7) of Van der Voo (1990) and reliability criteria of Meert et al. (2020). Italicized grades indicate that the paleomagnetic data of Strik (2004) is included in our new poles, which should be prioritized for database inclusion. b – baddeleyite; z – zircon; c – baked contact test; G – intraformational conglomerate test; F – intraformational fold test.

								Van der Voo (1990) Q								Meert et al. (2020) R									
Paleomagnetic Pole	Pole lat (°)	Pole long (°)	A95 (°)	Reference	Age	Method	Reference	1 - Age ±40 Ma	2 - Number/Stats	3 - Demagnetization/PCA	4 - Field Tests	5 - Structural Control	6 - Presence of Reversals	7 - Younger pole	Total	1 - Age ±15 Ma	2 - Techniques/Stats	3 - Rock Mag	4 - Field Tests	5 - Structural Control	6 - Reversal Test	7 - Younger pole	Total	Suggested Grade	Comments
Lower Package 0	4.4	89.9	6.7	this study (includes GHG P0 from Strik, 2004)	<2850 Ma >2772±2 Ma	SHRIMP-b	Hickman (2021) Wingate (1999)	0	1	1	0	1	0	1	4	0	1	0	0	1	0	1	3	B	Age constraints lax ~2850 to 2772±2. Lacking field stability test.
Strik Package 0	-1.5	93.6	8.2	Strik, 2004	<2850 Ma >2772±2 Ma	SHRIMP-b	Hickman (2021) Wingate (1999)	0	1	1	F	1	0	1	5	0	1	0	F	1	0	1	4	*B**	Age constraints lax ~2850 to 2772±2. Some data included in Lower Package 0 above
Upper Package 0	-8.3	115.6	13.7	this study	≥2772±2 Ma	SHRIMP-b	Wingate (1999)	1	1	1	0	1	0	1	5	1	0	0	0	1	0	1	3	B	Lacking field stability test.
Black Range Dyke Swarm	-3.8	130.4	15.0	Evans et al., 2017	2772±2 Ma	SHRIMP-b	Wingate (1999)	1	1	1	cG	1	0	1	6	1	1	0	cG	1	0	1	5	A	
Grand Mean Package 1	-43.0	161.2	7.1	this study (includes all P1 from Strik, 2004 and all Mt Roe Basalt from Schmidt & Embleton, 1985)	<2772±2 Ma >2762.51±0.68 Ma	SHRIMP-b ID-TIMS-z	Wingate (1999) this study	1	1	1	G	1	1	1	7	1	1	1	G	1	0	1	6	A	Sites from Schmidt & Embleton 1985 show reversed polarity but reversal test fails with C grade.
Strik Package 1	-41.4	158.5	2.7	Strik, 2004	<2772±2 Ma >2766±2	SHRIMP-b SHRIMP-z	Wingate (1999) Blake et al. (2004)	1	1	1	g	1	0	1	6	1	1	0	cG	1	0	1	5	*A**	Data included in GMP1 above
Strik Package 2	-41.5	157.3	12.5	Strik, 2004	2762.51±0.68 Ma	ID-TIMS-z	this study	1	1	1	0	1	0	0	4	1	1	0	0	1	0	0	3	B	Updated age constraint, Lacking field stability test.
Package 7 Volcano clastic	-33.7	179.1	7.9	this study	<2741±3 Ma >2721.57±0.64 Ma	SHRIMP-z ID-TIMS-z	Blake et al. (2004) this study	1	1	1	F	1	0	1	5	0	0	0	F	1	0	1	3	-	Further study recommended due to small number of samples and lithology
Package 7 Basalt	-56.3	140.0	7.0	this study (includes all NS and BCA P7 basalt from Strik, 2004)	>2721.57±0.64 Ma	ID-TIMS-z	this study	1	1	1	F	1	1	0	6	1	1	0	F	1	Rci	0	5	A	Overlapping poles Carboniferous to Permian
Strik Package 7	-56.2	140.2	10.1	Strik, 2004	2721±4 Ma	SHRIMP-z	Blake et al. (2004)	1	1	1	0	1	1	0	5	1	0	0	0	1	0	0	2	*B**	Lacking field stability test. Data included in P7 Basalt above. Overlapping poles Carboniferous to Permian
Package 8	-64.2	179.3	5.7	this study (includes all MC, NS, BCA P8 from Strik, 2004)	2720.52±0.80 Ma	ID-TIMS-z	this study	1	1	1	0	1	0	0	5	1	1	0	0	1	0	0	4	B	Partial unfold test inconclusive. Overlapping poles ~1600 Ma.
Strik Package 8	-68.9	182.1	10.3	Strik, 2004	2718±3 Ma	SHRIMP-z	Blake et al. (2004)	1	1	1	0	1	0	0	4	1	1	0	0	1	0	0	3	*B**	Lacking field stability test. Data included in P8 above. Overlapping poles ~1600 Ma
Strik MT	-43.8	201.2	3.7	Strik, 2004				0	1	1	0	1	0	0	3	0	1	0	0	1	0	0	2	x	No age constraint; not recommended for inclusion in databases.

Rci = reversal test with isolated observation & C grade
G = intraformational conglomerate test (primary)
F = intraformational fold test (primary)
b = baddeleyite
z = zircon
Required A grade criteria
Optional A grade criteria
Missing A grade criteria
g = conglomerate test
c = inverse baked contact test

(site JK1315) was found to be positive, following Watson (1956), with an R value of 4.8 less than the accepted cutoff of 6.98 for the 19 samples included (Fig. 8a), indicating that the Package 1 magnetization at GHG is primary. This test also meets the criteria for positive support of uniformly random directions in the Bayesian conglomerate test of Heslop & Roberts (2018).

While only ~15 km away from GHG, the lower half of the CR section (CR-East) yielded somewhat different paleomagnetic results. Basalt flows thought to represent Package 0 yielded a south to southeast and steeply dipping down ChRM direction, with a greater resemblance to Package 1 at both GHG and the upper half of CR than to Package 0. Both Schmidt and Embleton (1985) and Strik (2004) also found that the lower basaltic unit on the east side of the Marble Bar Basin gave directions more similar to Package 1 than the expected Package 0, and Strik (2004) grouped these eastern sites with Package 1. We similarly adopt this approach and interpret the slight directional offset from the other Package 1 directions (with ChRM directions southeast and steeply dipping down) to result from faulting through the section. The path of our measured section crosses two faults and an anticline through the sandstone unit, potentially indicating repeated stratigraphy. Radiometric K-Th-U imaging of the Pilbara shows that the lower half of the CR section bears the same signature as Package 1 in the rest of the Marble Bar Basin (Van Kranendonk et al., 2004), lending additional support for this interpretation.

The hyaloclastite breccia in the middle of the CR section yielded a negative conglomerate test (Fig. 8a). It failed the Watson (1956) conglomerate test, with an R value of 13.6 exceeding the allowed 5% significance level of 5.98. It also fails the Bayesian conglomerate test of Heslop & Roberts (2018). However, the ChRM direction obtained from these clasts is scattered around south with a moderate downward dip, similar to the CR-East basalt flows, potentially indicating that the negative test results from hydrothermal remagnetization during the penecontemporaneous emplacement of the Package 1 lava flows. The directions obtained for Package 1 basalt lava flows west of this breccia (CR-West) cluster well with those obtained from GHG, as well as with other Package 1 directions obtained by Strik (2004). We therefore group our three new stratigraphic section site means with site means obtained by Schmidt & Embleton (1985) and Strik (2004) from 6 other regions in the Pilbara to calculate a new grand mean direction for Package 1, with a VGP located at 43.0°S, 161.2°E, A_{95} = 7.1°, paleolatitude = 48.9° (9 regions, 64 sites, 450 samples).

4.2.2. Packages 7–8: Tumbiana Formation & Maddina Basalt

Samples from most of the volcaniclastic and basalt paleomagnetic sites across the Package 7–8 transition showed excellent stability to thermal demagnetization, primarily with single-component behavior and unblocking temperatures of 480 °C for the volcaniclastics in the lower part of the sections, and 568–580 °C for the basalts in the upper part of the sections (Fig. 6). There was mostly good clustering of characteristic remanent magnetization (ChRM) directions from each locality. Sites with samples exhibiting inconsistent ChRM directions are excluded from the calculated mean directions (JK1320, JK1423, with unblocking temperatures <300°), as are the calcareous sandstones and carbonates of JK1321, JK1328, and JK1424. These sedimentary units have unblocking temperatures of <340° and show a wide scatter of ChRM directions around the present local field. A low-temperature overprinting event is inferred.

The Package 7 volcaniclastic sediments at the base of the MCN and MCS sections yield northwest directions dipping moderately upward, in contrast to the overlying Package 7 basalt flows, which dip steeply south and down (Fig. 7). The Package 7 volcaniclastics are grouped into a separate site-level directional mean. Basalts sampled at MCN and MCS, along with other basalts sampled by Strik (2004) in the Meentheena Centrocline, Nullagine Syncline, and Boodalyeri Creek area, are grouped into a Package 7 basalt directional mean. We do not include the Package 7 paleomagnetic data obtained by Strik (2004) in the West Pilbara Basin because those samples were collected from strata continuously mapped as Kylena Basalt, which is classified by Blake (2001) as Package 6. Package 8 basalts sampled at MCN and MCS yielded a south to southeast, moderately downward dipping direction of ChRM, and we include Package 8 data from Strik (2004) in our mean direction.

We conducted fold tests as a field stability test on our three Package 7 and 8 directional groups to ascertain if these paleomagnetic directions resulted from primary magnetization. This test was made possible by the differing dips exhibited across the Meentheena Centrocline, compared to flat-lying sediments in the Nullagine Syncline and the Boodalyeri Creek area (Fig. 1a). For the Package 7 volcaniclastics, the fold test of Fisher et al. (1987) was strongly positive when comparing the ratio of k values to the 95% F-ratio value, while for Package 7 basalt and Package 8 this test was inconclusive. However, all three directional groups yielded the best clustering with varying degrees of partial unfolding, and partial fold tests for both Package 7 directional groups are positive at the 95% confidence level of Fisher et al. (1987) (Fig. 8b). For Package 7 volcaniclastics, a k_{max}/k_{geo} ratio of 12.4 is attained with 90% unfolding, though 70% unfolding also yields significantly better clustering than in-situ data and would also yield a positive test. For Package 7 basalts, a k_{max}/k_{geo} ratio of 3.2 is attained with 70% unfolding. For Package 8, the data clusters best with a partial unfolding of 60%, but a lower k_{max}/k_{geo} ratio of 1.85 falls below the 95% critical F-ratio value (Fig. 8b). Thus, we cannot reject the null hypothesis of a common k-value between geographic and 60% unfolded datasets, and this technically constitutes an inconclusive partial unfold test. But with improved clustering at 60–70% unfolding, this result still provides support for our interpretation of Package 7 and suggests deposition on primary slopes of ~ 5-10° through the duration of emplacement of Packages 7 and 8 and provides support for primary magnetization. We suggest that the Meentheena Centrocline was experiencing tectonic activity during the deposition of Packages 7 and 8; the consistency of stratigraphy, yet difference in thickness of the units we described, may lend support to this hypothesis. The pattern of enhanced clustering through successively greater degrees of unfolding as deposition continued is more indicative of a declination anomaly rather than inclination shallowing. Our interpretation of partial unfolding is also bolstered by performing bootstrap fold tests on these directional groups after Tauxe & Watson (1994). This approach shows the greatest clustering of directions at 25–115% unfolding for Package 7 volcaniclastics (a positive test), 60–90% unfolding for Package 7 basalts, and 32–83% unfolding for Package 8 (Fig. S2).

Following these fold tests, we present VGPs for each of these groups based on their peak values of partial unfolding. Package 7 volcaniclastics yield a VGP located at 33.7°S, 179.1°E, A_{95} = 7.9°, paleolatitude = -35.4° (5 sites, 35 samples; Fig. 9). For Package 7 basalts, the VGP is at 56.3°S, 140.0°E, A_{95} = 7.0°, paleolatitude = 51.5° (11 sites, 73 samples). For Package 8 basalts, the VGP is located at 64.2°S, 179.3°E, A_{95} = 5.7°, paleolatitude = 32.1° (14 sites, 94 samples).

Since the Package 7 volcaniclastic direction is of opposite polarity relative to all but one Package 7 basalt site, we attempted a reversal test of McFadden & McElhinny (1990) to test for a common mean direction between our Package 7 volcaniclastic and Package 7 basalt directional groups. This test failed at the 99.9% level, showing these directional groups were not sourced from a common mean direction, as is also shown by their offset VGPs. We also performed a reversal test between the one reversed basalt flow documented by Strik (2004) in the Boodalyeri Creek area versus our ten other Package 7 basalt sites. This test for an isolated observation was passed with C criteria – the distance between directions of 11.1° is less than the critical angle of 19.6° (McFadden & McElhinny, 1990). This analysis provides further support for a primary magnetization of Package 7 basalts.

4.3. Geochronology

The stratigraphic positions of each geochronology sample are shown with squares on Fig. 3. Colored squares represent samples that yielded

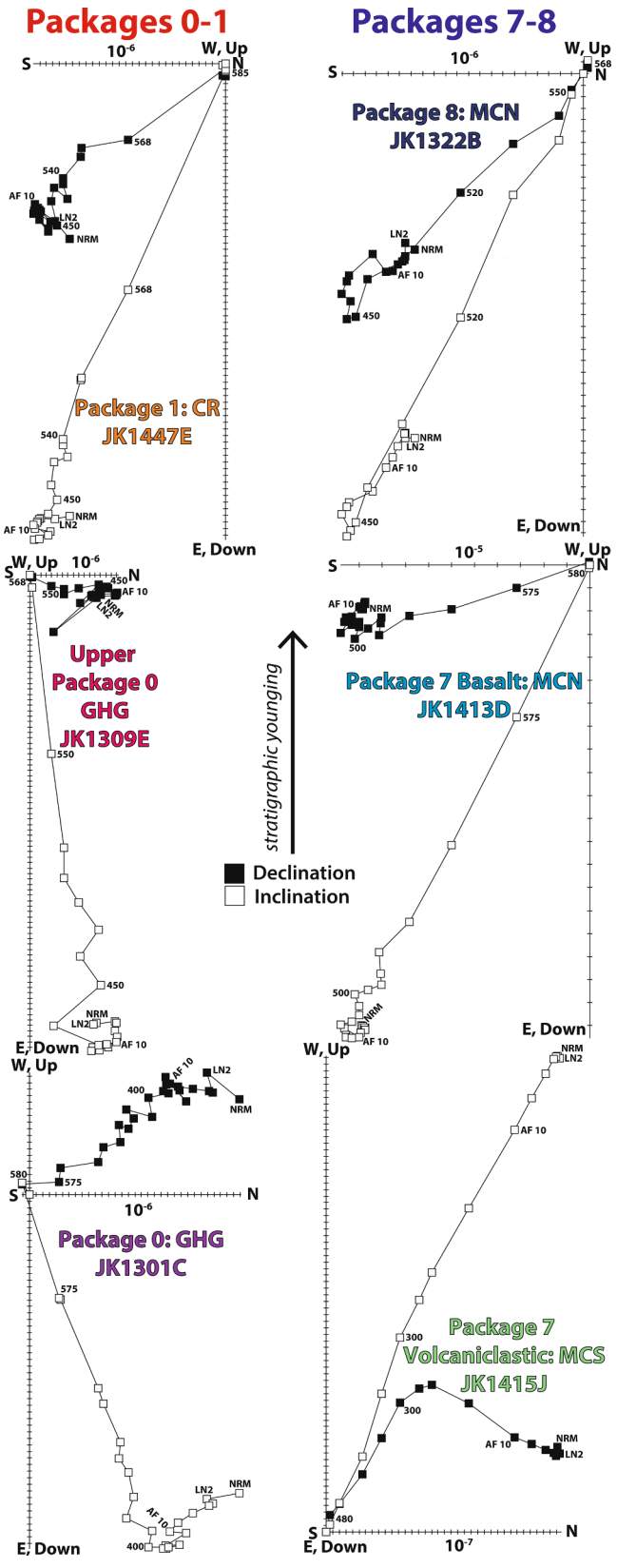

Fig. 6. Orthogonal projection diagrams of paleomagnetic samples. These plots show the demagnetization behavior of representative samples from each of the directional groups in this study; numbers indicate temperature steps. Diagrams use tilt-corrected coordinates. All other demagnetization data and plots are available on the MagIC database (link in Data Availability section).

zircon ages and are discussed below; greyed-out squares represent samples that either did not yield zircon or yielded only detrital or inherited grains. U-Pb data is found in Table S2. All geochronology samples collected in the Package 0–1 sections yielded only inherited ages of ~3.3 Ga (Table S2), the predominant age of granitoids in the region (Nelson, 2008). The distribution of zircon dates from GHG are shown in Figure S3. Photographs of samples collected and dated from Packages 7 and 8 are displayed in Fig. 5. Concordia plots with some zircon images from each sample are provided in Fig. 10. Weighted mean ages were calculated from overlapping individual zircon dates that overlapped with the Concordia line. A small number of grains with younger ages were excluded from weighted means because they are discordant or may have been affected by Pb-loss; some older grains were excluded because they appear to represent an earlier phase of crystallization. Ages are reported with 2σ uncertainties ± x/y/z, where x represents analytical uncertainty alone, y includes uncertainties in the ET-535 tracer used, and z includes all systematic uncertainties.

4.3.1. *Package 2: Spinaway Porphyry*

Sample J339 (21.76549°S, 129.091807°E) of massive quartz-feldspar porphyry was collected on Route 138 (Marble Bar Road) in the Nullagine Syncline (Fig. 1a), to serve as a minimum age for Package 0–1. This porphyry, part of the overlying Package 2 (Blake, 2001), is not found in the Marble Bar Basin, but we deemed it more likely to yield zircons than any of the interbeds collected in Packages 0–1. Thousands of zircons were separated from this sample, and they are semi-translucent, with some colorless and others orange. Zircons range in morphology from equant and small (<100 μm) to long (>200 μm) with pronounced termination points. Twenty-one were selected for analysis, and 14 were successfully dated. For this sample and others, a number of zircons were lost due to dissolution during chemical abrasion or zircon loss during chemistry; other analyses were unsuccessful due to discordance, high Pb blank relative to radiogenic Pb, or inheritance. Zircons range in age from 2767.1 ± 4.9 Ma to 2761.5 ± 2.1 Ma; all dates and ages reported in this paper are Th- and Pa-corrected $^{207}Pb/^{206}Pb$ ages. The weighted mean age of the sample is 2762.43 ± 0.58/0.59/6.9 Ma (MSWD = 0.44, n = 10). This age is somewhat offset and more precise than the prior SHRIMP zircon $^{207}Pb/^{206}Pb$ age radiometric age of 2766 ± 2 Ma obtained for the Spinaway Porphyry (Blake et al., 2004).

4.3.2. *Packages 7–8: Tumbiana Formation & Maddina Basalt*

Sample K295 (21.323106°S, 120.394508°E) was collected in the MCN section and is comprised of an accretionary lapilli tuff interbedded with the upper carbonates of the Meentheena Member, providing an age for uppermost Package 7. Lapilli were ~1 mm scale (Fig. 5f). Approximately 50 zircons were separated from this sample, and they were ~50 μm in size, opaque, equant, and slightly rounded. Twenty-seven were selected for analysis, and 8 were successfully dated. Zircons range in age from 2747.6 ± 2.0 Ma to 2717.5 ± 2.0 Ma; the isolated older age may be a xenocryst derived from the host rock of the tuff's magma chamber (Miller et al., 2007). The weighted mean age of the sample is 2721.23 ± 0.88/0.88/6.9 Ma (MSWD = 1.7, n = 4). This age overlaps with and improves precision on a SHRIMP age of 2721 ± 4 for a tuff 300 m into the volcaniclastic section of Package 7 in the Nullagine Syncline (Blake et al., 2004).

Samples K302 and K329 were collected from two different outcrops of 1 cm-scale accretionary lapilli tuff, that were along strike from each other at the same stratigraphic height and immediately overlying the uppermost Package 8 lava flow at MCN (Fig. 5h). For sample K302 (21.323551°S, 120.409556°E), which had a lower density of lapilli, approximately 100 zircons were separated from this sample, and they were euhedral, prismatic, blocky and opaque in appearance. Forty-one zircons were selected for analysis, and 14 were successfully dated. Zircons range in age from 2724.9 ± 3.0 Ma to 2718.7 ± 4.0 Ma. The weighted mean age is as 2721.12 ± 0.56/0.58/6.8 Ma (MSWD = 0.61, n = 12).

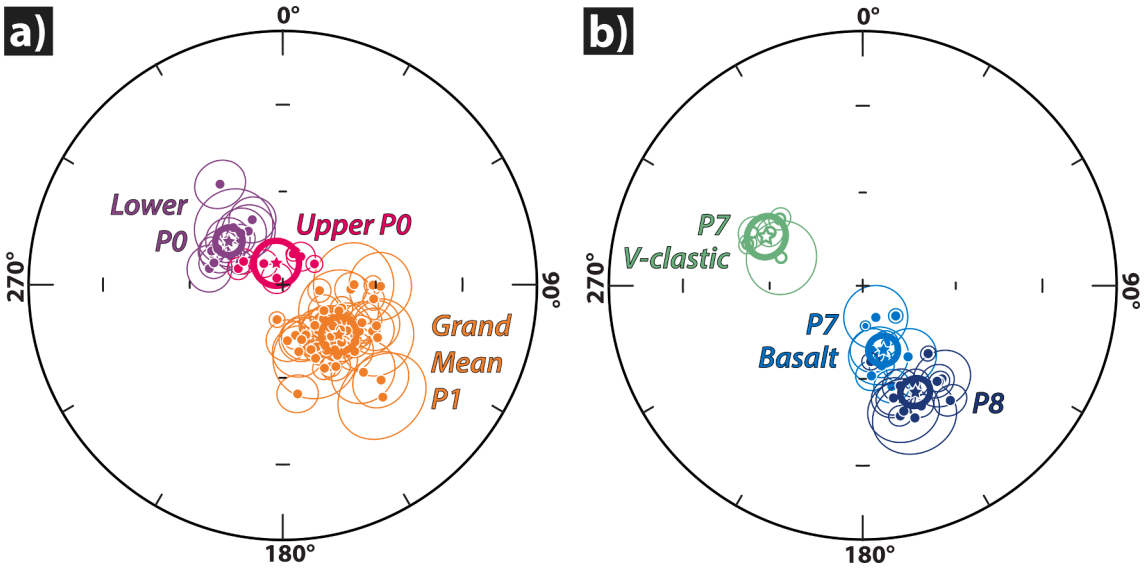

Fig. 7. Paleomagnetic site mean directions. These equal area plots show the site mean directions with α95 (thin circles) for all sites used in the calculation of a virtual geomagnetic pole for each directional group identified here. Groups are identified by color; the starred directions with thick circles indicate the directional group means with A95. The directions in (a) are all shown in 100% tilt-corrected coordinates; in (b), site means are shown with 90% partial unfolding for Package 7 volcaniclastics, 70% unfolding for Package 7 basalts, and 60% unfolding for Package 8. The open symbols for Package 7 volcaniclastics indicate upper hemisphere directions.

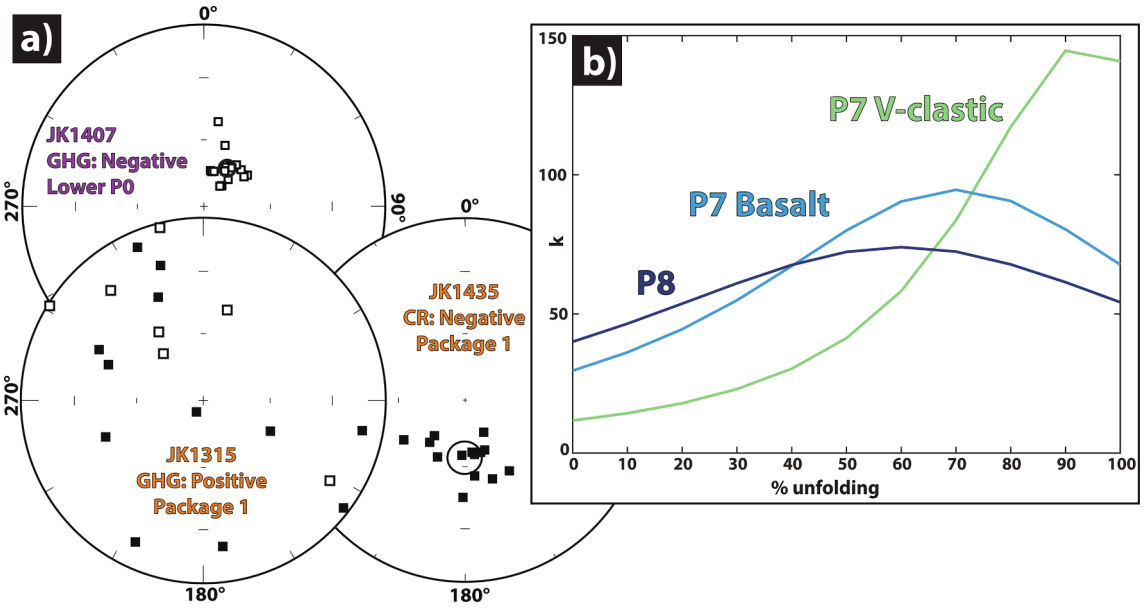

Fig. 8. Paleomagnetic field stability test results. (a) Equal area plots with tilt-correction show the result of conglomerate tests performed on the Bellary Formation conglomerate at the base of Package 0 (JK1407 at GHG) and Package 1 hyaloclastite breccias (JK1315 at GHG, JK1435 at CR). Scattered ChRM directions at JK1315 indicate a positive conglomerate test, and clustered directions at JK1407 (aligned with present local field) and JK1435 indicate failed tests. **(b)** Sequential fold tests on Package 7 volcaniclastics and basalts, and Package 8 indicate greatest clustering of directions (k) at 90% unfolding for the volcaniclastics, and 60–70% unfolding for the other groupings.

For sample K329 (21.323073°S, 120.413734°E), approximately 100 zircons were separated from this sample, and they are glassy, prismatic, and mostly euhedral in appearance, with half equant and half tabular morphologies. Thirty zircons were selected for analysis, and nine were successfully dated. Zircons range in age from 2724.5 ± 7.4 Ma to 2718.06 ± 0.90 Ma. The weighted mean age of the sample is 2721.33 ± 0.83/0.84/6.9 (MSWD = 1.9, n = 8). Our ages for K302 and K329 agrees well with each other, and with the SHRIMP age of 2718 ± 3 Ma obtained in an accretionary lapilli tuff interbedded with Package 8 lava flows in the Nullagine Syncline (Blake et al., 2004).

5. Discussion

Our stratigraphically constrained paleomagnetic and geochronological analyses of the Fortescue Group yield new high-quality poles for future inclusion in paleomagnetic databases, with implications for Pilbara plate motion during the Archean, Fortescue magmatism, and Neoarchean magnetic field reversals. These are detailed in the following sections.

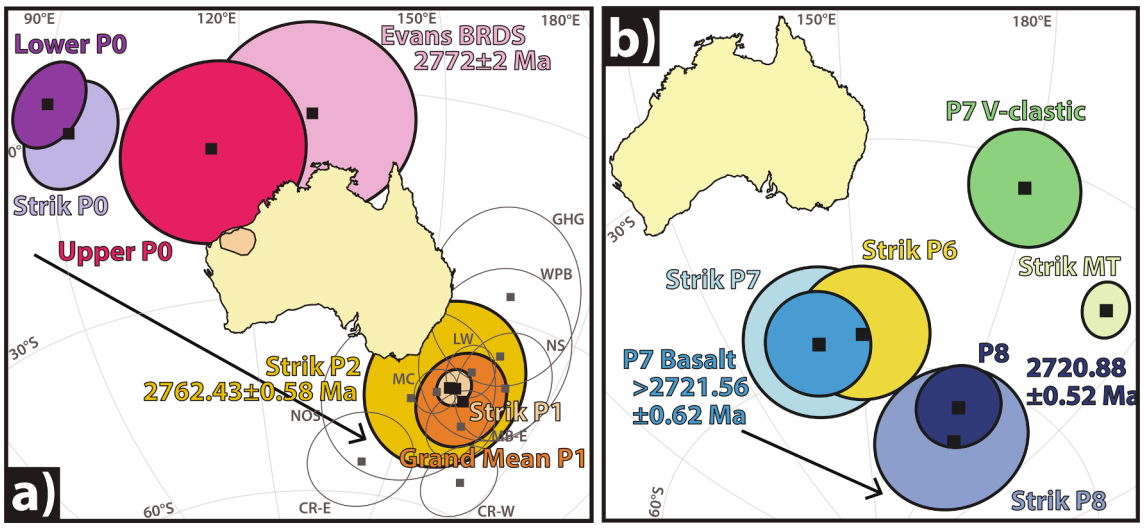

Fig. 9. Virtual geomagnetic poles. The mean paleomagnetic poles calculated in this study for the Pilbara craton (highlighted in pale orange and in present Australian coordinates) are shown in (a) for Packages 0–1, and (b) for Packages 7–8, compared to prior directions obtained by Strik (2004) and Evans et al. (2017). Pole ages are from this study except for that of the Black Range Dyke Suite (BRDS), which is from Wingate (1999). Arrows show the generalized younging direction of the apparent polar wander path. Site mean paleomagnetic data can be found in Table S1. (For interpretation of the references to color in this figure legend, the reader is referred to the web version of this article.)

5.1. *New high-quality Archean paleomagnetic poles for the Pilbara craton*

By yielding new paleomagnetic data and high-precision ages, our study updates the position and ages of five poles and provides one new pole that we propose for inclusion in databases of reliable paleomagnetic poles for Precambrian tectonic reconstructions (Evans et al., 2021). In Table 1, poles are graded based on the quality criteria of Van der Voo (1990) and the reliability criteria of Meert et al. (2020). We follow Evans

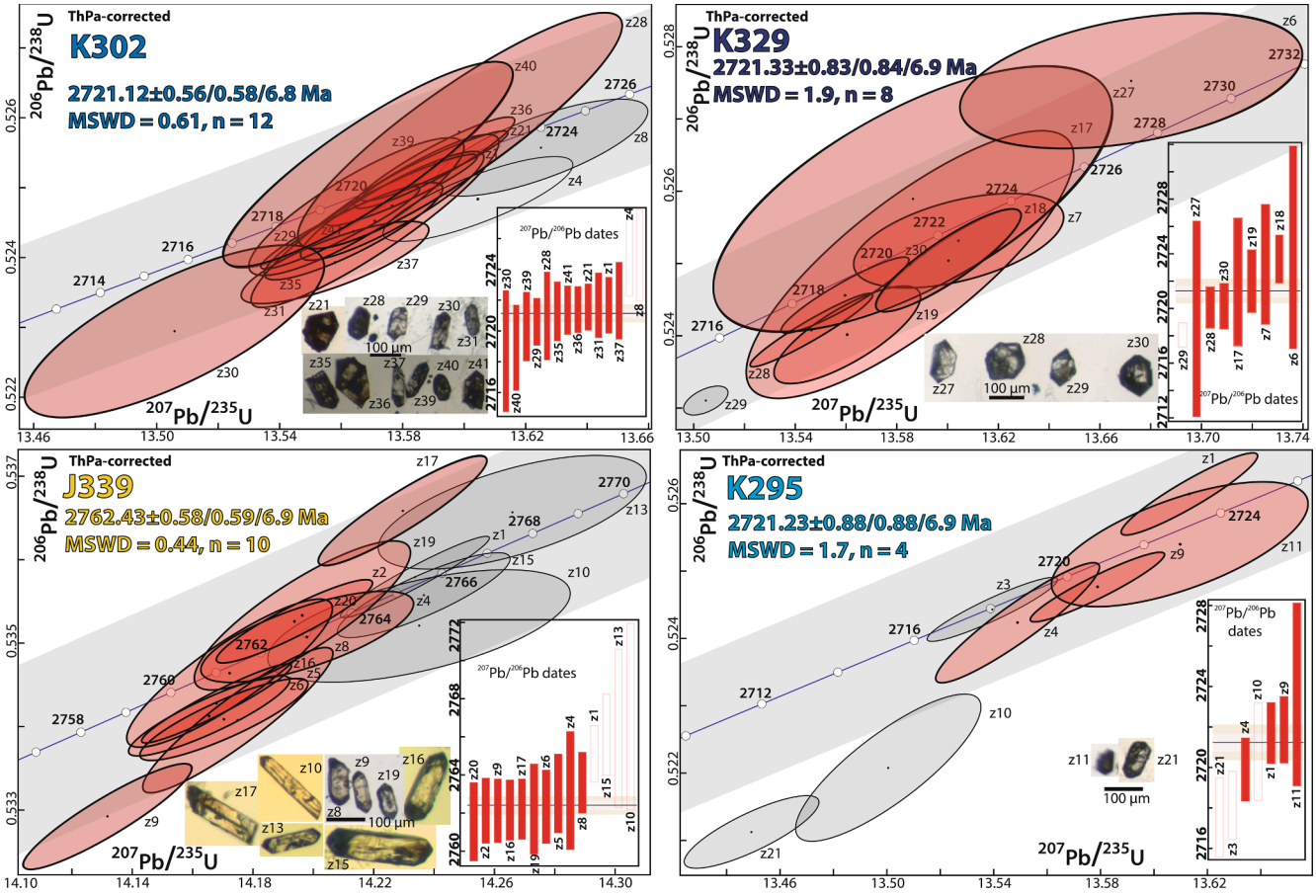

Fig. 10. Fortescue Group geochronology data. Concordia plots show new geochronology results from the Fortescue Group, with weighted mean ages and zircon images. Interception with the Concordia line indicates closed-system behavior. All U-Pb data can be found in Table S2.

et al. (2021) in suggesting that poles receive an A grade when they possess an age constrained within 40 Ma (Q1, not necessarily R1), a sufficient number and statistical quality of poles (Q2, not necessarily R2), demagnetization and principal component analysis (Q3), field stability tests (Q4, R4), and structural control (Q5, R5). Poles with B grade lack one or more of these criteria, and we highlight further work that would be needed for promotion to A grade.

While we were unable to obtain a direct age constraint on Package 0 in this study, its age can be loosely constrained to between 2850 Ma (the age of the Split Rock Suite, one of the youngest basement units in the East Pilbara Basin; Hickman, 2021) and the SHRIMP zircon age of 2772 ± 2 Ma (Wingate, 1999) obtained on the Black Range Dolerite Suite of dikes, described below. Because Strik (2004) was able to perform a fold test in Package 0, that pole could be promoted to an A classification if this age range were acceptable. Our Lower Package 0 pole would similarly benefit from a field stability test performed on these basalts; without one, we suggest that it be graded with a B classification, for which this loose age constraint may be acceptable.

The direction we obtain from Upper Package 0 overlaps with the paleomagnetic pole recently obtained for the Black Range Dolerite Suite (BRDS) of dykes (Evans et al., 2017), which have been previously correlated to the Mount Roe Basalt based on compatible but imprecise geochronology. A SHRIMP zircon study yielded ages of 2763 ± 13 Ma and 2775 ± 10 Ma for the Mount Roe Basalt (Arndt et al., 1991), a TIMS study on air-abraded zircons produced an age of 2767 ± 3 Ma for the Mount Roe Basalt (Van Kranendonk et al., 2006), and a SHRIMP baddeleyite study of the BRDS provided a weighted mean age of 2772 ± 2 Ma calculated from four different dikes in the BRDS (Wingate, 1999). Since weighted means should only be applied when events are interpreted to happen simultaneously, it could be argued that this age interpretation is inappropriate as individual dike dates ranged from 2774.7 ± 4.6 Ma to 2768.0 ± 5.6 Ma. Nevertheless, Evans et al. (2017) maintain that Wingate's age of 2772 ± 2 Ma is the best age estimate of the BRDS following additional ID-TIMS baddeleyite work on the suite, which yielded slightly younger ages that overlapped with the SHRIMP age. Zircon overgrowths were observed on the baddeleyite grains selected for TIMS work, potentially biasing the new ages too young (Evans et al., 2017). Given the overlapping position of the VGPs for the BRDS and Upper Package 0, the age of 2772 ± 2 Ma can therefore be applied to this portion of the Mount Roe Basalt; the other Mount Roe Basalt ages cannot be correlated unambiguously with our results, as they are either too imprecise or lack paleomagnetic identification of the sampled rocks to Package 0 or Package 1. With the addition of this crucial age constraint, we propose our Upper Package 0 pole for inclusion in future paleomagnetic databases with a B grade, since it lacks a field stability test.

Our Grand Mean Package 1 pole meets all seven quality criteria and six of seven reliability criteria, making it a suitable update for the Package 1 pole of Strik et al. (2003) currently included in the Evans et al. (2021) database and potentially meriting an A grade. We can constrain the age of these basalts to between 2772 ± 2 Ma and 2762.43 ± 0.58 Ma, using the BRDS age of Wingate (1999) and our new Package 2 age. Our conglomerate test on the hyaloclastite breccia was positive, and dual polarities were documented (Schmidt & Embleton, 1985). Schmidt & Embleton (1985) also assessed the magnetic mineralogy of the Mount Roe Basalt; they used electron microprobe analysis to observe 2–3 μm chromiferous magnetite grains in a chlorite host, with 10 μm grains of rutile, thus meeting the R3 reliability criterion of Meert et al. (2020). We have averaged paleomagnetic poles from nine different regions (poles are shown in grey in Fig. 8) into this Grand Mean pole, even though we recognize that there may be minor declination differences, secular variation, and local rotations among these different regions. These possible differences will not be resolved without further study.

We suggest that the Package 2 pole, based on the results of Strik et al. (2003) and included in Evans et al. (2021), be updated to include our higher-precision age constraint for Package 2, as well as the more robust statistics from other paleomagnetic sites sampled by Strik (2004). However, without a field stability test, this pole would retain a B classification.

Some uncertainty remains regarding the reversely magnetized Package 7 volcaniclastics. If a reversal occurred, its stratigraphic height would be between 140 and 230 m at MCN, or ~30 m at MCS. Strik (2004) observed sites with reversed polarity in Package 7 (from one basalt flow in the Boodalyeri Creek area and a correlated sill in the West Pilbara Basin), suggesting that the reversed polarity described here may be a reliable result, a possibility strengthened by the positive fold test we document here. However, there is a 20-40° offset in declination between these units and the Package 7 volcaniclastics. An alternative interpretation, possibly bolstered by the lower unblocking temperatures of the volcaniclastic units, is that these represent an overprinted direction. Strik (2004) described a "Medium Temperature" direction that is northwest and moderately inclined upward, but our results show a steeper inclination. The VGP we calculate for the Package 7 volcaniclastics is distant from the Package 7 basalts, as well as the results of Strik (2004) for Package 6–8 and "Medium Temperature" components (Fig. 9). Alternative explanations for this offset include age difference, paleosecular variation, or a magnetic field that differs from our assumption of a geocentric axial dipole. With these uncertainties, as well as a lack of age constraint, we do not propose including the Package 7 volcaniclastic paleomagnetic pole in paleomagnetic databases at this time.

While Evans et al. (2021) include grouped poles Packages 4–7 and Packages 8–10 (Strik et al., 2003) on their list of B poles, we have focused on Packages 7 and 8, and have calculated poles for those packages alone. Our Package 7 basalt pole would earn an A grade, as we supply a high-precision age constraint and a statistically positive partial unfold test at 70% unfolding. We suggest that the basalts are preserved as growth strata emplaced during regional tilting across the Meentheena Centrocline. Our Package 8 pole would earn a B grade with the improved age constraint we provide here, but lacks a statistically robust field stability test, as described above.

5.2. Rapid Neoarchean Pilbara plate motion?

There is a significant change in the paleogeography of the Pilbara craton during emplacement of the Package 0–1 Mount Roe Basalt flows. Between the lower and upper Package 0 directions, there is 25.5 ± 15.3° (2835 ± 1697 km) of displacement between the VGPs, and between Upper Package 0 and Package 1, there is 54.8 ± 15.4° (6092 ± 1716 km) of displacement between the VGPs (Fig. 9). Since all zircons dated from GHG and CR were inherited, a plate velocity across these two transitions cannot be calculated at this time.

The Pilbara craton moved from a paleolatitude of 50.8 ± 6.7° during Lower Package 0 emplacement, to 68.2 ± 15° for the BRDS and 76.3 ± 13.7° during Upper Package 0, and to 48.9 ± 7.1° during Package 1. We can attempt to constrain a minimum rate of the second portion of this motion, between the BRDS and Grand Mean Package 1, using the Wingate (1999) age of 2772 ± 2 Ma for BRDS and our new high-precision Package 2 age of the Spinaway Porphyry of 2762.43 ± 0.58 Ma, the latter used as a minimum conservative age estimate for Grand Mean Package 1. Following the approach of Swanson-Hysell et al. (2014), we use a Monte Carlo simulation to calculate a minimum rate of plate motion 23 ± 20 cm/a (Fig. 11a and b). This interpretation, which does not depend upon the craton crossing the polar circle, allows for a combination of local vertical axis rotation as well as translation. However, our model reveals that explaining the offset between poles through rotation alone (requiring negligible translation) is implausible, as that model would fall within the extreme lower tail of our confidence interval. We also note that 23 ± 20 cm/yr (and other rates described below) are minimum velocity estimates, as paleolongitude is not constrained in these calculations. Therefore, the rate of Pilbara plate motion we calculate between the BRDS and Grand Mean Package 1 poles is at

least comparable if not more rapid than the fastest plate motion observed on Earth today, of ~20 cm/a (Zahirovic et al., 2015).

In contrast to the hypothesis of vertical axis rotation described above, we can also calculate a rate for Pilbara plate motion that may have been dominated by translation (Fig. 11c and d). Evans et al. (2017) interpreted the sequence of VGPs from Package 0, Upper Package 0/BRDS, and Package 1 as translational plate motion of the Pilbara craton across the polar circle, rather than the block rotation advocated by Strik (2004). To assess this interpretation, we therefore update the Monte Carlo estimation described above to force cratonic motion across the pole. When we calculate the rate of motion between our Upper Package 0 (with the Wingate (1999) age of the overlapping BRDS pole) and Grand Mean Package 1 poles (with the same Package 2 age constraint as above) this interpretation yields a minimum translational rate of 64 ± 23 cm/a (Fig. 10). We also calculate this rate using individual BRDS dike ages obtained by Wingate (1999) and estimate a rate 51.5 ± 25.8 cm/a when the oldest dike age of 2774.7 ± 4.6 Ma is applied to Upper Package 0, and a rate of ~32 m/a when the youngest dike age of 2768.0 ± 5.6 Ma is applied. The latter rate is extraordinarily fast because the lower precision SHRIMP age nearly overlaps with our TIMS age for Package 2. Whether the oldest individual BRDS age or the BRDS weighted mean age of 2772 ± 2 is applied to our Upper Package 1 pole, the rate of Pilbara plate motion we calculate over this interval far exceeds any plate motion observed on Earth today.

Between VGPs for Package 7 basalt and Package 8, we calculate a displacement of 19.4 ± 9.0° (2157 ± 1004 km; Fig. 8), which falls between the initial estimate of Strik et al. (2003) of 27.2° of movement across this interval and a revised estimate by Strik (2004) of a 14.4° shift. Our only geochronology sample from Package 7, K295, overlies the Package 7 basalt paleomagnetic site and overlaps in age with our results from Package 8, and thus does not provide a meaningful constraint on the plate velocity for this interval. Even though none of the lapilli tuffs we sampled at MCN or MCS in the lowermost volcaniclastic unit of Package 7 yielded zircons, it may be fruitful to sample this lithology in other regions with the goal of obtaining an improved age constraint for Package 7 and an updated plate velocity estimate for this interval.

Our calculated minimum velocities calculated for the Pilbara, as it drifted and/or rotated across the polar circle from the Upper Package 0 to Package 1 position, are noteworthy not only because they exceed modern plate tectonic rates, but also because they are far greater than the average plate velocities calculated for the Pilbara craton during the Mesoarchean (Brenner et al., 2020). For that older interval, minimum velocities are calculated using only three poles with ages ca. 3350, 3180, and 2800 Ma. We suggest that such long-term averages could be overlooking shorter intervals of more rapid motion. While any combination of a hotter Archean Earth with more rapid mantle convection, or more rapid true polar wander, have been invoked previously as possible explanations for rapid drift rates, our results show that Archean plate velocities were not uniformly fast or decreasing monotonically as time progressed.

5.3. Is the Fortescue Group a large igneous province?

With an estimated basaltic volume of 250,000 km^3 (Thorne & Trendall, 2001), the Fortescue Group invites comparison to other continental flood basalt provinces, such as the Columbia River Basalt Group or the Deccan Traps. Indeed, the basaltic volume of the Fortescue Group is 20% greater than that of the Columbia River Basalt Group (Reidel, 2015). However, Thorne & Trendall (2001) object to the classification of the Fortescue Group as a continental flood basalt due to its paleoenvironment and duration of its emplacement. While the northern exposures of the Fortescue Group suggest predominantly subaerial, 'continental' emplacement, the basalts of the southern Fortescue Group are predominantly subaqueous, as if they erupted in a passive continental margin. Also, the Fortescue Group's emplacement duration of ~60 Ma is far longer than that of any other flood basalt described (Thorne & Trendall, 2001).

In recent decades, large igneous provinces (LIPs) have been defined more broadly to include a wider array of geologic expressions of voluminous magmatism, such as oceanic LIPs and silicic LIPs. Therefore, the subaqueous emplacement and more felsic geochemistry of the Fortescue basalts would not preclude the classification of the Fortescue as a large igneous province. However, the 60 Ma duration of Fortescue emplacement would be its most notable disqualifying factor, as LIPs should be emplaced within a short duration (<5 Ma), or with multiple short pulses over a maximum of a few 10 s of Ma (Ernst & Youbi, 2017). A recent review of high-precision geochronology of large igneous provinces finds that thus far, all well-dated LIPs were emplaced in <1 Ma (Kasbohm et al., 2021).

Since the Fortescue Group contains three distinct basaltic formations (Mount Roe, Kylena, and Maddina Basalts), perhaps each of these could be considered an individual LIP. Volume estimates for these units are 72,000 km^3, 68,000 km^3, and 110,000 km^3 respectively (Thorne & Trendall, 2001), though these may be hampered by limited geologic preservation. While the Mount Roe and Kylena Basalts do not satisfy the >100,000 km^3 volume cutoff for LIP classification, the Maddina Basalt (Packages 8–10) could qualify as a continental flood basalt with its larger volume. Our geochronology shows a minimum duration of 0.98 ± 1.03 Ma for the emplacement of Package 8 at MCN, suggesting that the rest of the Maddina Basalt could have been emplaced in a few Ma or less.

While the Fortescue Group may or may not meet specific criteria for LIP classification, assessing its emplacement dynamics may yield insights for an early prototype of LIP magmatism. One aspect of more recent LIP emplacement that is not always well-known is the relative timing of intrusive and extrusive magmatism (Kasbohm et al., 2021). By contrast, our paleomagnetic correlation showing the temporal coincidence of the Mount Roe Basalt flows of Upper Package 0 and the intrusive activity of the BRDS conclusively places the widespread BRDS within the temporal and stratigraphic context of the Fortescue Group, and allows for a temporal correlation between dikes and lava flows.

Another crucial aspect of LIP emplacement to consider is the duration of hiatuses. The Package 1–10 subdivisions of Blake (2001) were initially envisioned to be bounded by significant time breaks in the Fortescue stratigraphy. Our geochronology sampling at the boundary between Packages 7 and 8 yield the first high-precision temporal constraints on one of these hiatuses, since K295 is in the uppermost Package 7, and K302 overlies the Maddina Basalts in Package 8. While Blake (2001) noted the Package 7–8 boundary was likely relatively short (1–5 Ma), and subsequent geochronology produced a duration of ~3 Ma (Blake et al., 2004), we show that the time elapsed between these two samples (whose dates overlap within uncertainty) is 0.98 ± 1.03 Ma, suggesting that the actual amount of time elapsed before Package 8 volcanism started is much less. Therefore, it seems that time breaks between these packages is less significant than previously thought, and we cannot preclude the possibility that the contact between Packages 7 and 8 may in fact be conformable.

5.4. Neoarchean magnetic field reversals

Our results from the Fortescue Group yields insights into the timing of magnetic field reversals and duration of polarity chrons during the Archean. Strik (2003) documented Earth's oldest known magnetic field reversal between Packages 1 and 2, which we now constrain with a minimum age of 2762.11 ± 0.66 Ma on the Spinaway Porphyry, and the previously existing maximum age of 2772 ± 2 Ma from the BRDS (Evans et al., 2017; Wingate, 1999). With limited stratigraphic context, it is difficult to assess whether the reversely magnetized Package 1 lava flows sampled in the West Pilbara Basin by Schmidt & Embleton (1985) and Strik (2004) constitute an additional, earlier reversal, or if they represent an earlier, Package 1-aged onset of the reversal currently defined by Package 2.

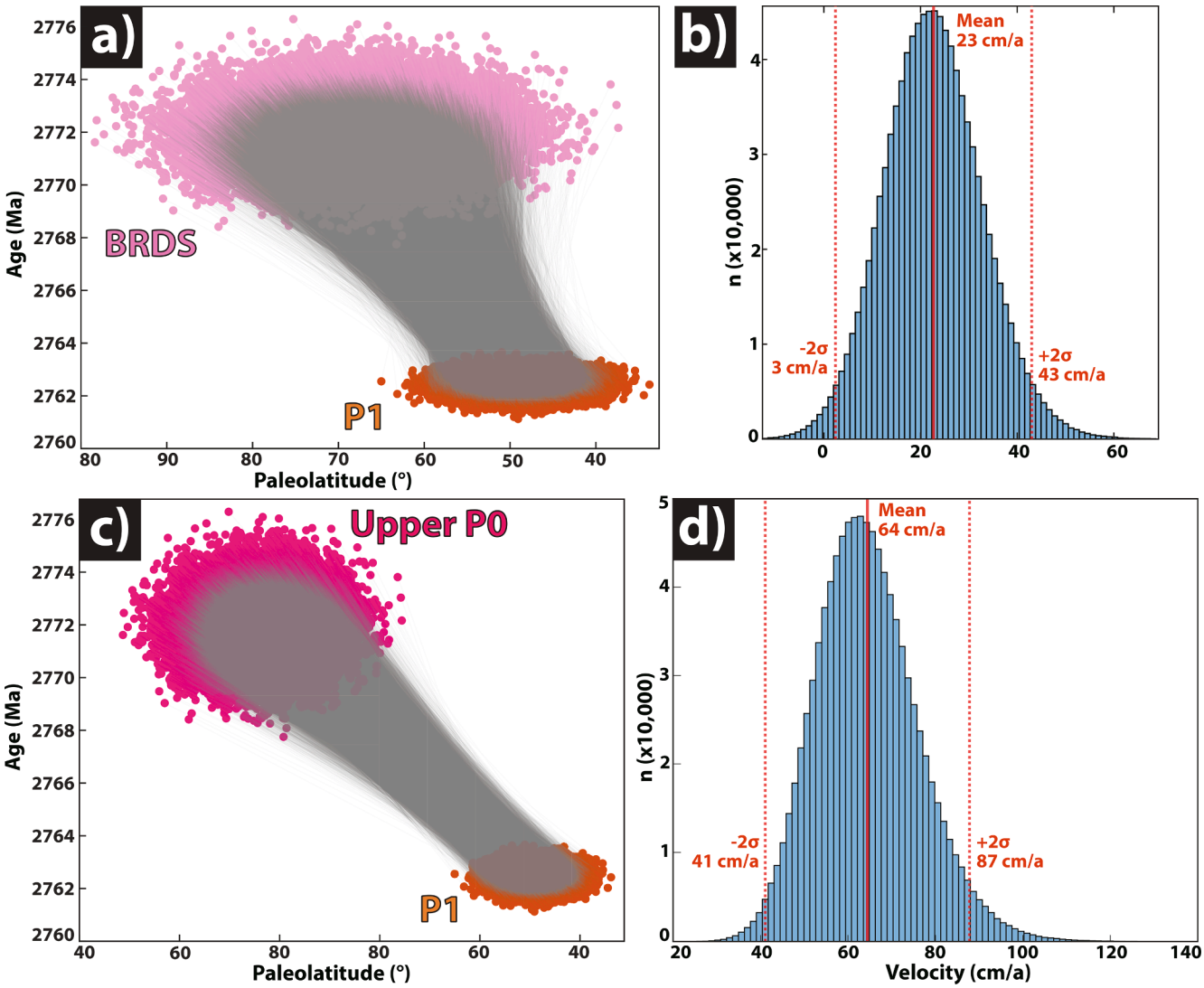

Fig. 11. Monte Carlo simulation of Pilbara craton plate velocity. (a) To provide velocity constraints between the BRDS and Package 1 that permit translation and rotation, possible ages based on geochronology are plotted against paleolatitudes permitted by our paleomagnetic data. The pink and orange points, connected by grey lines showing displacement rates during this interval, demonstrate 50,000 of the 1 million simulated pairs. (b) A histogram shows the 1 million simulated rates with the mean and 95% confidence intervals identified with red lines for (a). (c) To estimate translational motion between Upper Package 0 and Package 1 that crosses the pole, as interpreted by Evans et al. (2017), we repeat the simulation in (a) but with paleolatitudes mirrored about the 90° polar value. (d) A histogram shows the 1 million simulated rates with the mean and 95% confidence intervals identified with red lines for (c). (For interpretation of the references to color in this figure legend, the reader is referred to the web version of this article.)

While polarity reverts to normal after Package 2, the reversely magnetized basalt flow in the Boodalyeri Creek Area sampled by Strik (2004) suggest that an additional reversed polarity interval occurred during Package 7, in the Tumbiana Formation, at ~2722 Ma. The reversely magnetized Package 7 volcaniclastic sediments we sample at the base of MCN and MCS may also may document this interval, if their directions are interpreted to be primary. Normal polarity returns at or before 2721.57 ± 0.64, based on our zircon age from the Tumbiana stromatolites overlying the normally magnetized basalts. These data suggest that Earth's polarity reversed at least four times between 2772 and 2721 Ma. The durations of each polarity chron defined would potentially be ~10 Ma during the Package 2 reversed interval, ~40 Ma during the normal chron when Packages 3–6 were deposited, and ~1 Ma for the reversed interval in Package 7. The pattern of the long normal chron (during the deposition of Packages 3–6) followed by the brief reversed interval in Package 7 reflects patterns in other thick and densely sampled Precambrian successions, where long intervals (30–40 Ma) of uniform polarity are juxtaposed with intervals of rapid reversals (Elston et al., 2002; Gallet et al., 2012; Pavlov & Gallet, 2010). This alternation between reversing and non-reversing regimes may reflect the sensitivity of the geodynamo to changing heat flux patterns at the core-mantle boundary, in a time prior to the crystallization of the inner core (Gallet et al., 2012).

6. Conclusions

By using a stratigraphic approach to integrate paleomagnetic and high-precision geochronological data from the Fortescue Group, we provide crucial new constraints on plate velocities, large igneous province magmatism, and magnetic field reversals in the Neoarchean. We present six new high-quality paleomagnetic poles and four high-precision U-Pb ages that show that the Pilbara craton drifted at a minimum rate of 23 ± 20 to 64 ± 23 cm/a (depending on the extent of cratonic rotation versus translation) over an interval of ~10 million years in the Neoarchean. Both rates far exceed both background drift rates for the craton, and modern rates of plate motion. Our new age of 2721.23 ± 0.88/0.88/6.9 Ma for the Tumbiana Formation provides the

first high-precision U-Pb zircon age constraint interbedded within a colony of Archean stromatolites. The new constraints described here on plate tectonic rates, timing of magmatism, and magnetic field reversals show how an early prototype of a large igneous province may enlighten future investigations of its successors.

CRediT authorship contribution statement

Jennifer Kasbohm: Conceptualization, Formal analysis, Investigation, Visualization, Writing - original draft, Writing - review & editing. **Blair Schoene:** Conceptualization, Investigation, Resources, Writing – review & editing, Supervision, Funding acquisition. **Scott A. Maclennan:** Investigation, Writing – review & editing. **David A.D. Evans:** Validation, Formal analysis, Writing – review & editing. **Benjamin P. Weiss:** Conceptualization, Resources, Writing – review & editing.

Declaration of Competing Interest

The authors declare that they have no known competing financial interests or personal relationships that could have appeared to influence the work reported in this paper.

Data availability

All paleomagnetic data has been uploaded to the Magnetics Information Consortium (MagIC), and is accessible at this link: https://earthref.org/MagIC/19607.

Acknowledgements

We thank A. Campion, A. Maloof, and E. Bolton for assistance in the field, and R. Fu for support in the MIT Paleomagnetism Lab. Z. Gong provided a helpful review of an earlier version of this manuscript, and J. Biasi gave advice on uploading data to MagIC. We thank two anonymous referees for their constructive feedback in peer review. This material is based upon work supported by the NSF Graduate Research Fellowship under grant no. DGE-1656466 and was funded by Princeton University Department of Geosciences.

Appendix A. Supplementary material

Supplementary data to this article can be found online at https://doi.org/10.1016/j.precamres.2023.107114.

References

Arndt, N.T., Nelson, D.R., Compston, W., Trendall, A.F., Thorne, A.M., 1991. The age of the Fortescue Group, Hamersley Basin, Western Australia, from ion microprobe zircon U-Pb results. Aust. J. Earth Sci. 38 (3), 261–281. https://doi.org/10.1080/08120099108727971.

Blake, T.S., 1984. The Lower Fortescue Group of the northern Pilbara craton: stratigraphy and palaeogeography. Arch. Proterozoic Basins Pilbara: Evol. Mineral. Potential 9, 123–143.

Blake, T.S., 1993. Late Archaean crustal extension, sedimentary basin formation, flood basalt volcanism and continental rifting: the Nullagine and Mount Jope Supersequences, Western Australia. Precambr. Res. 60 (1–4), 185–241. https://doi.org/10.1016/0301-9268(93)90050-C.

Blake, T.S., 2001. Cyclic continental mafic tuff and flood basalt volcanism in the Late Archaean Nullagine and Mount Jope supersequences in the eastern Pilbara, Western Australia. Precambr. Res. 107 (3–4), 139–177. https://doi.org/10.1016/S0301-9268(00)00135-2.

Blake, T.S., Buick, R., Brown, S.J.A., Barley, M.E., 2004. Geochronology of a Late Archaean flood basalt province in the Pilbara Craton, Australia: constraints on basin evolution, volcanic and sedimentary accumulation, and continental drift rates. Precambr. Res. 133 (3–4), 143–173. https://doi.org/10.1016/j.precamres.2004.03.012.

Blättler, C.L., Kump, L.R., Fischer, W.W., Paris, G., Kasbohm, J.J., Higgins, J.A., 2017. Constraints on ocean carbonate chemistry and p<inf>CO2</inf>in the Archaean and Palaeoproterozoic. Nat. Geosci. 10 (1) https://doi.org/10.1038/ngeo2844.

Bowring, J.F., McLean, N.M., Bowring, S.A., 2011. Engineering cyber infrastructure for U-Pb geochronology: Tripoli and U-Pb-Redux. Geochem. Geophys. Geosyst. 12 (6) https://doi.org/10.1029/2010GC003479.

Brenner, A.R., Fu, R.R., Evans, D.A.D., Smirnov, A.V., Trubko, R., Rose, I.R., 2020. Paleomagnetic evidence for modern-like plate motion velocities at 3.2 Ga. Sci. Adv. 6 (17), 1–10. https://doi.org/10.1126/sciadv.aaz8670.

Brown, M., Johnson, T., Gardiner, N.J., 2020. Plate tectonics and the Archean Earth. Annu. Rev. Earth Planet. Sci. 48 (1), 1–30. https://doi.org/10.1146/annurev-earth-081619-052705.

Claiborne, L. L., Miller, C. F., Gualda, G. A. ., Carley, T. L., Covey, A. K., Wooden, J. L., Fleming, M.A., 2018. Zircon as magma monitor: robust,temperature-dependent partition coefficients from glass and zircon surface and rim measurements from natural systems. In: Moser, D.E., Corfu, F., Darling, J. R., Reddy, S. M., Tait, K. (Eds.), Microstructural Geochronology: Planetary Records Down to Atom Scale (1st ed., pp. 3–33).

Condon, D.J., Schoene, B., McLean, N.M., Bowring, S.A., Parrish, R.R., 2015. Metrology and traceability of U-Pb isotope dilution geochronology (EARTHTIME Tracer Calibration Part I). Geochim. Cosmochim. Acta 164, 464–480. https://doi.org/10.1016/j.gca.2015.05.026.

Davies, G.F., 1992. On the emergence of plate tectonics. Geology 20 (11), 963–966. https://doi.org/10.1130/0091-7613(1992)020<0963:OTEOPT>2.3.CO;2.

Elston, D.P., Enkin, R.J., Baker, J., Kisilevsky, D.K., 2002. Tightening the Belt: Paleomagnetic-stratigraphic constraints on deposition, correlation, and deformation of the Middle Proterozoic (ca. 1.4 Ga) Belt-Purcell Supergroup, United States and Canada. Bull. Geol. Soc. Am. 114 (5), 619–638. https://doi.org/10.1130/0016-7606(2002)114<0619:TTBPSC>2.0.CO;2.

Ernst, R.E., Youbi, N., 2017. How Large Igneous Provinces affect global climate, sometimes cause mass extinctions, and represent natural markers in the geological record. Palaeogeogr. Palaeoclimatol. Palaeoecol. 478, 30–52. https://doi.org/10.1016/j.palaeo.2017.03.014.

Evans, D. A. D., Pesonen, L. J., Eglington, B. M., Elming, S.-Å., Gong, Z., Li, Z.-X., et al., 2021. An expanding list of reliable paleomagnetic poles for Precambrian tectonic reconstructions. In: Ancient Supercontinents and the Paleogeography of Earth, Elsevier, pp. 605–639. 10.1016/B978-0-12-818533-9.00007-2.

Evans, D.A.D., Smirnov, A.V., Gumsley, A.P., 2017. Paleomagnetism and U-Pb geochronology of the Black Range dykes, Pilbara Craton, Western Australia: a Neoarchean crossing of the polar circle. Aust. J. Earth Sci. 64 (2), 225–237. https://doi.org/10.1080/08120099.2017.1289981.

Fisher, R.A., 1953. Dispersion on a sphere. Proc. R. Soc. Lond. A 217 (1130), 295–305.

Fisher, N.I., Lewis, T., Embleton, B.J.J., 1987. Statistical Analysis of Spherical Data. Cambridge University Press.

Gallet, Y., Pavlov, V., Halverson, G., Hulot, G., 2012. Toward constraining the long-term reversing behavior of the geodynamo: A new "Maya" superchron ~1 billion years ago from the magnetostratigraphy of the Kartochka Formation (southwestern Siberia). Earth Planet. Sci. Lett. 339–340, 117–126. https://doi.org/10.1016/j.epsl.2012.04.049.

Gerstenberger, H., Haase, G., 1997. A highly effective emitter substance for mass spectrometric Pb isotope ratio determinations. Chem. Geol. 136 (3–4), 309–312. https://doi.org/10.1016/S0009-2541(96)00033-2.

Heslop, D., Roberts, A.P., 2018. A Bayesian approach to the paleomagnetic conglomerate test. J. Geophys. Res. Solid Earth 123 (2), 1132–1142. https://doi.org/10.1002/2017JB014526.

Hickman, A.H., 2010. Marble Bar. In Western Australia Geological Survey 1:250 000 Geological Map Sheet SF 50-8 (3rd ed.). Perth, WA.

Hickman, A.H., 2021. East Pilbara Craton : a record of one billion years in the growth of Archean continental crust. East Perth, Western Australia.

Hulot, G., Finlay, C.C., Constable, C.G., Olsen, N., Mandea, M., 2010. The magnetic field of planet Earth. Space Sci. Rev. 152 (1–4), 159–222. https://doi.org/10.1007/s11214-010-9644-0.

Jaffey, A.H., Flynn, K.F., Glendenin, L.E., Bentley, W.C., Essling, A.M., 1971. Precision measurement of half-lives and specific activities of ^{235}U and ^{238}U. Phys. Rev. C 4 (5), 1889–1906. https://doi.org/10.1103/PhysRevC.4.1889.

Jones, C.H., 2002. User-driven integrated software lives: "PaleoMag" paleomagnetics analysis on the Macintosh. Comput. Geosci. 28 (10), 1145–1151.

Kasbohm, J.J., Schoene, B., Burgess, S.D., 2021. Radiometric constraints on the timing, tempo, and effects of large igneous province emplacement. In: R. E. Ernst, A. J. Dickson, & A. Bekker (Eds.), Large Igneous Provinces: A Driver of Global Environmental and Biotic Changes (pp. 27–82). American Geophyiscal Union and John Wiley and Sons, Inc. 10.1002/9781119507444.ch2.

Kasbohm, J.J., Schoene, B., 2018. Rapid eruption of the Columbia River flood basalt and correlation with the mid-Miocene climate optimum. Sci. Adv. 4 (9), 1–8. https://doi.org/10.1126/sciadv.aat8223.

Kirschvink, J.L., 1980. The least-squares line and plane and the analysis of palaeomagnetic data. Geophys. J. R. Astron. Soc. 62 (3), 699–718. https://doi.org/10.1111/j.1365-246X.1980.tb02601.x.

Kirschvink, J.L., Kopp, R.E., Raub, T.D., Baumgartner, C.T., Holt, J.W., 2008. Rapid, precise, and high-sensitivity acquisition of paleomagnetic and rock-magnetic data: Development of a low-noise automatic sample changing system for superconducting rock magnetometers. Geochem. Geophys. Geosyst. 9 (5).

Korenaga, J., 2003. Energetics of mantle convection and the fate of fossil heat. Geophys. Res. Lett. 30 (8), 1–4. https://doi.org/10.1029/2003GL016982.

Krogh, T.E., 1973. A low-contamination method for hydrothermal decomposition of zircon and extraction of U and Pb for isotopic age determinations. Geochim. Cosmochim. Acta 37 (3), 485–494. https://doi.org/10.1016/0016-7037(73)90213-5.

Lipple, S.L., 1975. Definitions of new and revised stratigraphic units of the eastern Pilbara region. Annual Report–Western Australia, Department of Mines, 1974, 98–103.
Mattinson, J.M., 2005. Zircon U-Pb chemical abrasion ("CA-TIMS") method: combined annealing and multi-step partial dissolution analysis for improved precision and accuracy of zircon ages. Chem. Geol. 220 (1–2), 47–66. https://doi.org/10.1016/j.chemgeo.2005.03.011.
McFadden, P.L., McElhinny, M.W., 1990. Classification of the reversal test in palaeomagnetism. Geophys. J. Int. 103 (3), 725–729. https://doi.org/10.1111/j.1365-246X.1990.tb05683.x.
McLean, N.M., Bowring, J.F., Bowring, S.A., 2011. An algorithm for U-Pb isotope dilution data reduction and uncertainty propagation. Geochem. Geophys. Geosyst. 12 (6) https://doi.org/10.1029/2010GC003478.
McLean, N.M., Condon, D.J., Schoene, B., Bowring, S.A., 2015. Evaluating uncertainties in the calibration of isotopic reference materials and multi-element isotopic tracers (EARTHTIME Tracer Calibration Part II). Geochim. Cosmochim. Acta 164, 481–501. https://doi.org/10.1016/j.gca.2015.02.040.
Meert, J.G., Pivarunas, A.F., Evans, D.A.D., Pisarevsky, S.A., Pesonen, L.J., Li, Z.X., et al., 2020. The magnificent seven: a proposal for modest revision of the Van der Voo (1990) quality index. Tectonophysics 790 (March), 228549. https://doi.org/10.1016/j.tecto.2020.228549.
Miller, J.S., Matzel, J.E.P., Miller, C.F., Burgess, S.D., Miller, R.B., 2007. Zircon growth and recycling during the assembly of large, composite arc plutons. J. Volcanol. Geoth. Res. 167 (1–4), 282–299. https://doi.org/10.1016/j.jvolgeores.2007.04.019.
Nelson, D.R., 2008. Geochronology of the Archean of Australia. Aust. J. Earth Sci. 55 (6–7), 779–793. https://doi.org/10.1080/08120090802094135.
Nier, A.O., 1950. A redetermination of the relative abundances of the isotopes of carbon, nitrogen, oxygen, argon, and potassium. Phys. Rev. 77 (6), 789–793. https://doi.org/10.1103/PhysRev.77.789.
Pavlov, V., Gallet, Y., 2010. Variations in geomagnetic reversal frequency during the Earth's middle age. Geochem. Geophys. Geosyst. 11 (1), n/a-n/a. https://doi.org/10.1029/2009gc002583.
Pidgeon, R., 1984. Geochronological constraints on early volcanic evolution of the Pilbara Block, Western Australia. Aust. J. Earth Sci. 31 (2), 237–242.
Reidel, S.P., 2015. The Columbia River Basalt Group: a flood basalt province in the Pacific Northwest, USA. Geosci. Can. 42, 151–168. https://doi.org/10.1007/s13398-014-0173-7.2.
Schmidt, P.W., Embleton, B.J.J., 1985. Prefolding and overprint magnetic signatures in Precambrian (~2.9–2.7 Ga) Igneous rocks from the Pilbara Craton and Hamersley Basin, NW Australia. J. Geophys. Res. 90 (B4), 2967. https://doi.org/10.1029/JB090iB04p02967.
Strik, G.H.M.A., 2004. Palaeomagnetism of late Archaean flood basalt terrains: implications for early Earth geodynamics and geomagnetism. Universiteit Utrecht.
Strik, G.H.M.A., Blake, T.S., Zegers, T.E., White, S.H., Langereis, C.G., 2003. Palaeomagnetism of flood basalts in the Pilbara Craton, Western Australia: Late Archaean continental drift and the oldest known reversal of the geomagnetic field. J. Geophys. Res. 108 (B12), 1–21. https://doi.org/10.1029/2003jb002475.
Swanson-Hysell, N.L., Vaughan, A.A., Mustain, M.R., Asp, K.E., 2014. Confirmation of progressive plate motion during the Midcontinent Rift's early magmatic stage from the Osler Volcanic Group, Ontario, Canada. Geochem. Geophys. Geosyst. 15 (5), 2039–2047. https://doi.org/10.1002/2013GC005180.
Swanson-Hysell, N.L., Ramezani, J., Fairchild, L.M., Rose, I.R., 2019. Failed rifting and fast drifting: Midcontinent Rift development, Laurentia's rapid motion and the driver of Grenvillian orogenesis. GSA Bull. 131 (5–6), 913–940. https://doi.org/10.1130/B31944.1.
Tauxe, L., Watson, G.S., 1994. The fold test: an eigen analysis approach. Earth Planet. Sci. Lett. 122 (3–4), 331–341. https://doi.org/10.1016/0012-821X(94)90006-X.
Thorne, A., Trendall, A., 2001. Geology of the Fortescue Group, Pilbara Craton, Western Australia. Bull. Geol. Surv. Western Australia 144.
Trendall, A.F., 1975. Preliminary geochronological results from two Pilbara porphyry bodies. Western Austr. Geol. Surv. Ann. Rep. 103–106.
Van der Voo, R., 1990. The reliability of paleomagnetic data. Tectonophysics 184 (1), 1–9. https://doi.org/10.1016/0040-1951(90)90116-P.
Van Kranendonk, M.J., Collins, W.J., Hickman, A., Pawley, M.J., 2004. Critical tests of vertical vs. horizontal tectonic models for the Archaean East Pilbara Granite-Greenstone Terrane, Pilbara Craton, Western Australia. Precambr. Res. 131, 173–211. https://doi.org/10.1016/j.precamres.2003.12.015.
Van Kranendonk, M.J., Bleeker, W., Ketchum, J., 2006. Phreatomagmatic boulder conglomerates at the tip of the ca 2772 Ma Black Range dolerite dyke, Pilbara Craton, Western Australia. Aust. J. Earth Sci. 53 (4), 617–630. https://doi.org/10.1080/08120090600686777.
Van Kranendonk, M.J., Smithies, R.H., Hickman, A.H., Champion, D., 2007. Review: secular tectonic evolution of archean continental crust: interplay between horizontal and vertical processes in the formation of the Pilbara Craton, Australiara. Terra Nova 19 (1), 1–38.
Watson, G.S., 1956. A test for randomness of directions. Geophys. Suppl. Monthly Notices Roy. Astronom. Soc. 7 (4), 160–161.
Wingate, M.T.D., 1999. Ion microprobe baddeleyite and zircon ages for Late Archaean mafic dykes of the Pilbara Craton, Western Australia. Aust. J. Earth Sci. 46 (4), 493–500. https://doi.org/10.1046/j.1440-0952.1999.00726.x.
Zahirovic, S., Müller, R.D., Seton, M., Flament, N., 2015. Tectonic speed limits from plate kinematic reconstructions. Earth Planet. Sci. Lett. 418, 40–52. https://doi.org/10.1016/j.epsl.2015.02.037.